

Supernova implosion-explosion in the light of catastrophe theory

Pierre-Henri Chavanis¹, Bruno Denet², Martine Le Berre³, and Yves Pomeau⁴ .

¹ Laboratoire de Physique Théorique (UMR 5152 du CNRS), Université Paul Sabatier, 118 route de Narbonne, 31062 Toulouse Cedex 4, France

² Université Aix-Marseille, IRPHE, UMR 7342 CNRS et Centrale Marseille, Technopole de Château-Gombert, 49 rue Joliot-Curie, 13384 Marseille Cedex 13, France.

³ ISMO-CNRS, Université Paris-Saclay, 91405 Orsay Cedex, France.

⁴ Ladhyx, Ecole polytechnique, 91128 Palaiseau, France.

September 10, 2019

Abstract. The present understanding of supernova explosion of massive stars as a two-step process, with an initial gravitational collapse toward the center of the star followed by an expansion of matter after a bouncing on the core, meets several difficulties. We show that it is not the only possible one: a simple model based on fluid mechanics, catastrophe theory, and stability properties of the equilibrium state shows that one can have also a *simultaneous* inward/outward motion in the early stage of the instability of the supernova described by a dynamical saddle-center bifurcation. The existence of this simultaneous inward/outward motion is sensitive to the model in such systems with long-range interactions. If a constant temperature is assumed (canonical ensemble), an overall inward motion occurs, but if one imposes with the same equation of state the constraint of energy conservation (microcanonical ensemble) there is an inward velocity field near the center of the star together with an outward velocity field in the rest of the star. We discuss the expansion stage of the remnants away from the collapsed core, and propose a new explanation for the formation of shock waves in the ejecta which differs from the usual Sedov-Taylor self-similar description.

PACS. 05.00.00 – 47.00.00 – 97.00.00

1 Introduction

In theoretical papers, the sudden death of massive stars is associated to at least two different processes, depending essentially on their mass (and secondarily on their composition, rotation speed...). Stars with masses in the range of $8 - 40 M_{\odot}$ die by a supernova phenomenon, which means that they partially explode. This phenomenon is presently described as an initial collapse toward the center of the star, *followed by* a violent expulsion of the outer layers of the star, leading to the observed supernovae. The death of more massive stars, or hypernovae, is believed to be a total collapse of the star into a black hole, without explosion (or a very faint one) but accompanied by gamma ray bursts. Although those phenomena are the most spectacular ones displayed to us in the Universe, their understanding remains a challenge. Among the many unsolved problems, we focus here on core-collapsing supernovae which go with the emission of matter and radiation by explosion. The collapse, which is not directly observed, is a phenomenon which has been the subject of many theoretical studies since several decades, including more and more detailed physics, although the observed explosion is still a controversial topic because it requires to explain how to reverse the velocity field of the first stage collapse. Despite exten-

sive hydrodynamical simulations, the reversal of the motion from inward (collapse or *implosion*) to outward (the observed *explosion* of supernovae) is not yet explained because it requires very large outward directed forces to turn the tide. According to most works on core collapse supernovae, this reversal is due to a stiffening of the equation of state at the center, which stops the collapse and leads to a bounce. An outward propagating shock is created at this moment but, typically, in numerical studies this shock stalls at some definite radius except if it is revived by some mechanism (see [1] and more recently [2] with references herein). Neutrino heating is often invoked but numerical simulations have shown that this is not generally sufficient to produce an explosion. More recently, 3D hydrodynamic instabilities have been discussed but they are still highly controversial. In summary, the revival of the stalled accretion shock remains an unexplained process since 1980 and, as written by Burrows [2], the understanding of these phenomena is “in an unsatisfactory state of affairs” and could remain so until the state of nuclear matter inside a star can be reproduced on Earth or a close enough (but not too close!) supernova is observed.

In the present work we use the same approach as in [3] (Paper I) where we definitely do not consider the im-

mensely complex nuclear processes taking place in a star, but we propose to describe the star as a dynamical system subject to a loss of stability just before it dies. The starting point of our theory is the fact that stars die abruptly in a matter of seconds while they evolve on a very long time, in the billion years range. Similar stability losses with very different time scales occur in other dynamical systems in nature. The difference of time scales was recently proposed as a tool for predicting natural catastrophes before they happen, because it has been shown that one may define in certain cases a precursor time which stands in between the very short and very long time scales [4,5]. It was shown that this precursor time exists for systems loosing their stability via a *dynamical* saddle-node bifurcation, dynamical in the sense that the crossing of the bifurcation results from a slow sweeping of the bifurcation across a saddle-node, that requires a parameter changing slowly with time. This time dependence of the parameter can be hidden into the original equations as in the case of creeping of soft solids and sleep-wake transitions. The validity of this approach was confirmed [6] by experiments and by mathematical models consisting in coupled ordinary differential equations (ODE)'s (the nature of the bifurcation in the case of earthquakes is still an open question [7, 8]). In these studies, a universal equation was derived for the order parameter close to the bifurcation, which is first order in time because these systems are dissipative and reduce to the van der Pol equation in the relaxation limit. In the case of supernovae we may anticipate that they likely belong to the class of dynamical catastrophes because of the very different time scales involved, but we expect that the universal equation describing the slow-fast transition should be of second order in time because the system is non-dissipative (we consider compressible inviscid fluids, at least in the early stage of the dynamics). Therefore, the normal form should be associated to a saddle-center bifurcation¹ in place of a saddle-node. Moreover, we expect to obtain spatial information like density and velocity profiles at the critical point, in addition to the time evolution of the amplitude, because our models consist in coupled partial differential equations (PDE)'s.

To describe the star, we use here, as in Paper I, simple fluid mechanical models based on the Euler-Poisson equations (with gravity) and a particular equation of state. We show first that the equilibrium state of such a star may undergo a saddle-center bifurcation. Then, we study the dynamical solution close to the critical point in the weakly nonlinear regime where we derive the normal form. Finally, we describe the strongly nonlinear regime where we show that the solution displays a self-similar behavior. What differs here from Paper I concerns the choice of the time dependent parameter. While in Paper I we considered a fluid with temperature $T(t)$ slowly decreasing with time, here we consider that the control parameter is the energy $E(t)$. This amounts to going from a canonical description (given temperature) to a microcanonical one

(given energy). The interesting result is that this simple change of thermodynamical ensemble leads to very different dynamics, as pointed out in previous studies concerning phase transitions in self-gravitating N -body systems (see the review in [9]). These studies were launched in view of applications to astrophysics where galaxies, globular clusters, self-gravitating dust gas (supposed to be at the origin of planet formation), and fermions gases (like electrons in white dwarfs, neutrons in neutrons stars, or massive neutrinos in dark matter models) are examples of self-gravitating systems. Using tools of thermodynamics and statistical mechanics, it was found that very different dynamics characterize canonical and microcanonical ensembles, especially in the vicinity of phase transitions. In general, a single collapsed core is formed in the canonical case, whereas a collapsed core surrounded by a halo is formed in the microcanonical case. Therefore, a question naturally arises: what should be obtained with the fluid model of Paper I when passing from the canonical description which leads to a total collapse of the star with a growing singularity at its core, to the microcanonical one?

Following the same procedure as in Paper I, we show that the microcanonical Euler-Poisson (MEP) model provides some generic properties that are identical to those of the canonical Euler-Poisson (CEP) model, but there also exist very important differences that drastically change the outcome. We show first that the loss of equilibrium occurs here via a saddle-center bifurcation, as in Paper I. In both models, the bifurcating solution reduces to the Painlevé I equation which describes the time dependence of the amplitude of the spatial mode in the weakly nonlinear regime that we call the Painlevé regime although Painlevé equations were neither derived nor studied in the context of bifurcation theory before our work to the best of our knowledge. During this regime, the important difference between the canonical and the microcanonical models concerns the radial dependence of the neutral mode (in particular the velocity field) which reflects the loss of balance between the inward pull of self-gravity and the outward pull of pressure. This loss of balance (which *a priori* depends on the location in the star) is global. Therefore, if the spatial profile of the velocity displays different directions, it will remain so, at least in the early stage of the Painlevé regime. In Paper I, the gravity was found to be dominant everywhere in the star with respect to the pressure, whereas here the gravity is not dominant everywhere. That gives different orientations of the radial velocity as a function of the radius. More precisely, we show that the microcanonical situation turns the all inward-going velocity field (found in the canonical case, see Paper I) into a velocity directed inward near the center of the star and outward in the rest of the star. This shows that in a simple model, fair to study because of the many uncertainties on what *really* happens in supernovae, one somehow gets rid of the difficulty of reversing an inward collapse of the star. Here, the early stage dynamics does already show a region where an outward going velocity motion is formed from the very beginning of the supernova process. More-

¹ A saddle-center bifurcation occurs when a center merges with a saddle at the fold point in Hamiltonian systems, a fairly standard situation as documented in Paper I.

over, as soon as matter flows outward, the attraction of the outer shell by the core gets smaller, and is unable to reverse the outward motion as we numerically observe.

We use, as in Paper I, an equation of state of the form $P(r, t) = T(t)g[\rho(r, t)]$, where P is the pressure and r the radial distance from the center of the star. This equation of state characterizes a barotropic system and describes compression and expansion processes including heat transfer. Such a model is likely unrealistic with respect to the great complexity of all processes taking place inside a star experiencing supernova explosion. Nevertheless, we argue that the reality depends on so many uncontrolled and poorly understood physical phenomena not realizable in laboratory experiments, and on initial conditions not well defined, that it seems a better way to try to solve a simple model in a, what we believe, completely correct way. Moreover, our choice of the function $g[\rho(r, t)]$ gives a finite mass to the star that avoids the box trick encountered in previous studies [9], where the self-gravitating particles are supposed to be confined within a spherical box, a device proposed by Antonov [10] for globular clusters. This trick was used because a stellar system has the tendency to evaporate under the effect of encounters between stars [11, 12, 13, 14], these encounters yielding a huge negative potential energy which acts as a source for the evaporation of the low energy stars located in the surrounding halo. The infinite mass problem is also encountered in the case of purely isothermal stars, and this is why we use a modified equation of state that is isothermal in the core and polytropic in the halo (with a polytropic index $n = 1$ or $\gamma = 2$) so that the density vanishes at a finite radius.

The paper is organized as follows. In Section 2, we present the MEP model and its equilibrium solutions. We show that such a *microcanonical* description of a star having a given constant energy E presents a saddle-center bifurcation in its dynamics. In Section 3, we show that the normal form of the MEP model close to the saddle-center bifurcation takes the form of Painlevé I equation and we compare the analytical prediction derived from it with a numerical simulation of the full MEP model. After the Painlevé regime, the full numerical study presented in Section 4 displays a self-similar behavior of the core before the singularity (core collapse) with exponents characterizing the dominance of gravity over pressure in this region, whereas the outward motion of the rest of the star continues to accelerate, but with a smaller velocity than the inward central motion. In Section 5, we study the dynamics just after the singularity where a self-similar solution is given for both parts of the star, the core domain which condensates by free fall, and the halo supposed to expand freely, these different dynamics being ruled by the respective importance of gravity and pressure forces. In Section 6, we consider the expansion of the remnants supposed to be well separated from the core. Assuming that the ejecta motion is isentropic, we show first that no self-similar solution exists when the condition of conservation of kinetic energy in the halo is imposed, because it makes too many conditions to be satisfied. We point out that this free expansion stage evolves naturally toward a non-self-similar

solution displaying shocks. This is because in this regime the velocity field obeys a Burgers-type equation as soon as gravity and pressure terms become negligible in the Euler equation. This approach differs fundamentally from the current description of shocks created by the collision with the interstellar medium (the Sedov-Taylor regime invoked in the literature). Here shocks are created by the interactions inside the halo, not with external matter, as soon as the initial velocity field is maximum somewhere inside the halo. In Section 7, and also throughout the paper, we compare the microcanonical results of the present study with the canonical results of Paper I, thereby illustrating the notion of ensembles inequivalence for systems with long-range interactions. Preliminary results of our study were presented in Ref. [15].

2 Saddle-center bifurcation in the microcanonical description of a self-gravitating fluid

We study the loss of equilibrium of a self-gravitating object (a star) in the framework of the hydrodynamical Euler-Poisson equations for an inviscid compressible fluid.

In Paper I, we considered the canonical description: the temperature T of the whole star was assumed to be fixed. This description amounts to considering the star as a system in contact with a thermostat, its energy $E(t)$ being not fixed. We considered an equation of state $P(\rho)$ presenting a saddle-center at a critical temperature T_c as the temperature decreases slowly. At this transition point two equilibrium solutions (one stable, the other unstable) merge, leading to a loss of equilibrium of the system since no equilibrium state exists for $T < T_c$. We studied the collapse of the star in the weakly nonlinear regime (Painlevé regime) near $T = T_c$ and next in the fully nonlinear regime.

Here, we consider the same model but for a closed (isolated, without thermostat) fluid, namely with fixed energy E , that corresponds to the *microcanonical* description. In that case, the temperature $T(t)$, which defines the internal energy $\frac{3}{2}Nk_B T(t)$ in equation (5), is not a fixed variable. Indeed, the fixed quantity at a given time is the total energy E , including kinetic energy, internal energy and gravitational energy. We consider the same equation of state $P(\rho)$ as in Paper I and show that it presents a saddle-center at a critical energy E_c . At that point, two equilibrium solutions (one stable, the other unstable) merge, leading to a loss of equilibrium of the system since no equilibrium state exists for $E < E_c$. Then, we assume that the energy $E(t)$ slowly/adiabatically decreases around the critical value E_c at which the saddle-center bifurcation occurs. The slow decrease of the energy could schematically describe the radiative process of the star burning its matter. We study the collapse of the star in the weakly nonlinear regime (Painlevé regime) and in the fully nonlinear regime. We compare the results with those obtained in the canonical ensemble.

2.1 Description of the microcanonical model

We use the same notations as in Paper I. The MEP model presented below differs from the CEP model by an added equation imposing the conservation of energy in the fluid, although this energy changes slowly because of added small losses. This constraint modifies the properties of the equilibrium states with noticeable consequences concerning the loss of equilibrium of the star. Some relations that are needed in our theoretical study are regrouped in Appendices A and B.

2.1.1 Euler-Poisson equations with conservation of energy

Let us recall the basic equations written first with the original physical variables. The Euler-Poisson system is

$$\frac{\partial \rho}{\partial t} + \nabla \cdot (\rho \mathbf{u}) = 0, \quad (1)$$

$$\frac{\partial \mathbf{u}}{\partial t} + (\mathbf{u} \cdot \nabla) \mathbf{u} = -\frac{1}{\rho} \nabla P - \nabla \Phi, \quad (2)$$

$$\Delta \Phi = 4\pi G \rho, \quad (3)$$

where $\mathbf{u}(\mathbf{r}, t)$ is the fluid velocity, $\rho(\mathbf{r}, t)$ the mass density, $P(\mathbf{r}, t)$ the pressure, G Newton's constant, and $\Phi(\mathbf{r}, t)$ the gravitational potential. We consider an equation of state of the so-called barotropic form

$$P = T(t)g(\rho), \quad (4)$$

namely with a uniform temperature. In equation (4), P and ρ depend on time and space, whereas $T(t)$ is a sort of spatial average of the temperature which only depends on time. We assume that the temperature $T(t)$ evolves in time, while remaining spatially uniform, so as to conserve the total energy (kinetic + thermal + gravitational). We consider a simple energetic constraint of the form

$$E = \frac{1}{2} \int \rho \mathbf{u}^2 d\mathbf{r} + \frac{3}{2} N k_B T(t) + \frac{1}{2} \int \rho \Phi d\mathbf{r} \quad (5)$$

which determines the temperature $T(t)$ for a given energy E . In doing so, we are assuming infinite thermal conductivity. This is a rough approximation making simpler the theoretical analysis.

2.1.2 Steady state of the Euler-Poisson equations in physical variables

It is convenient to introduce the enthalpy per unit mass h defined by $dh = dP/\rho$. For a barotropic equation of state of the form (4), the enthalpy is a function of the density $h(\rho) = \int^\rho [P'(\rho')/\rho'] d\rho'$. It is defined up to an additive constant. We impose $h(\rho = 0) = 0$ which determines the

constant. With this choice, the enthalpy vanishes at the edge of the star. Therefore,

$$h(\rho) = \int_0^\rho \frac{P'(\rho')}{\rho'} d\rho'. \quad (6)$$

In terms of the enthalpy, the momentum equation can be rewritten as

$$\frac{\partial \mathbf{u}}{\partial t} + (\mathbf{u} \cdot \nabla) \mathbf{u} = -\nabla h - \nabla \Phi. \quad (7)$$

The condition of hydrostatic equilibrium is

$$\nabla h + \nabla \Phi = \mathbf{0}. \quad (8)$$

Therefore, at equilibrium, $h(\mathbf{r}) = -\Phi(\mathbf{r}) + C$ where C is a constant. This is the Gibbs relation. We call r_0 the radius of the star at equilibrium and take $\Phi(+\infty) = 0$. On the boundary of the star, we have $h(r_0) = 0$ and $\Phi(r_0) = -GM/r_0$. Therefore, $C = -GM/r_0$ so that

$$h(\mathbf{r}) = -\Phi(\mathbf{r}) - \frac{GM}{r_0}. \quad (9)$$

From equations (4) and (6), we have $\rho = \rho(h, T)$. Taking the divergence of equation (8) and using the Poisson equation (3), we obtain the following differential equation for h

$$\Delta h + 4\pi G \rho(h, T) = 0. \quad (10)$$

2.1.3 Equation of state : an isothermal core with a polytropic envelope

To close the MEP model, we complete equations (1)-(5) by taking the same equation of state as in Paper I, namely

$$P(\rho, T) = \rho_* \frac{k_B T}{m} \left(\sqrt{1 + \rho/\rho_*} - 1 \right)^2. \quad (11)$$

This equation of state has an isothermal core ($P \sim \rho k_B T/m$ at large density $\rho \gg \rho_*$) and a polytropic halo ($P \sim K \rho^\gamma$ with $K = k_B T/4m\rho_*$ and $\gamma = 2$ at small density $\rho \ll \rho_*$) that confines the system in a finite region of space. Because of the isothermal core, we infer that the equation of state (11) should lead to a saddle-center bifurcation [16, 17, 18]. For the equation of state (11), the enthalpy (6) is explicitly given by

$$h(\rho, T) = 2 \frac{k_B T}{m} \ln \left(1 + \sqrt{1 + \rho/\rho_*} \right) - 2 \frac{k_B T}{m} \ln(2). \quad (12)$$

The inverse relation writes

$$\rho(h, T) = 4\rho_* \left(e^{mh/k_B T} - e^{mh/2k_B T} \right). \quad (13)$$

2.1.4 Dimensionless variables

In the following, it will be convenient to use dimensionless variables. The parameters regarded as fixed are ρ_* , M , m , k_B , and G . From ρ_* and M we can construct a length $L = (M/\rho_*)^{1/3}$. Then, we introduce the dimensionless quantities

$$\begin{aligned} \tilde{\rho} &= \frac{\rho}{\rho_*}, \quad \tilde{r} = \frac{r}{L}, \quad \tilde{\Phi} = \frac{\Phi}{G\rho_*L^2}, \quad \tilde{\mathbf{u}} = \frac{\mathbf{u}}{L\sqrt{G\rho_*}}, \\ \tilde{T} &= \frac{k_BT}{mG\rho_*L^2}, \quad \tilde{E} = \frac{E}{\rho_*GL^5}, \quad \tilde{P} = \frac{P}{GL^2\rho_*^2}, \quad \tilde{t} = t\sqrt{G\rho_*}. \end{aligned} \quad (14)$$

Working with the dimensionless variables with tildes amounts to taking $G = \rho_* = M = m = k_B = 1$ in the initial equations, a choice that we shall make in the following.

2.2 Equilibrium solutions, energy-radius relation, and caloric curve

For a given value of the energy (and therefore of the temperature) the steady state (equilibrium) is given by equations (10) and (13). The solutions may be expressed in terms of a second set of scaled variables, $\hat{r} = r/T^{1/2}$, $\hat{\rho} = \rho$, $\hat{\Phi} = \Phi/T$, $\hat{h} = h/T$, $\hat{p} = p/T$, $\hat{M} = M/T^{3/2}$ that leads to the following ODE for the steady state enthalpy

$$\hat{h}_{,\hat{r}^2} + \frac{2}{\hat{r}}\hat{h}_{,\hat{r}} + 4\pi\hat{\rho}(\hat{h}) = 0 \quad (16)$$

with the density-enthalpy relation

$$\hat{\rho}(\hat{h}) = 4(e^{\hat{h}} - e^{\hat{h}/2}). \quad (17)$$

As in Paper I, this equation is solved for a given value of $\hat{h}(0) = \hat{h}_0$, the only free parameter, with initial conditions $\hat{h}_{,\hat{r}}(0) = \hat{h}_{,\hat{r}^3}(0) = 0$ and $\hat{h}_{,\hat{r}^2}(0) = -(2\pi/3)\hat{\rho}(\hat{h}_0)$. The scaled radius of the star \hat{r}_0 corresponds to the smallest root of $\hat{h}(\hat{r}_0) = 0$. The scaled mass of the star $\hat{M} = \int_0^{\hat{r}_0} \hat{\rho}(\hat{r}, t) 4\pi\hat{r}^2 d\hat{r}$ is related to the temperature by the relation $\hat{M} = T^{-3/2}$ (we recall that the mass of the star is 1 with the units defined in Section 2.1.4). Using $\hat{r}_0 = r_0/T^{1/2}$ and the relation $\hat{M}(\hat{r}) = -\hat{r}^2\hat{h}_{,\hat{r}}$ (see Appendix A.1) yielding $\hat{h}_{,\hat{r}}(\hat{r}_0) = -1/(\sqrt{T}r_0^2)$, we obtain

$$r_0 = \left[\frac{\hat{r}_0}{-\hat{h}_{,\hat{r}}(\hat{r}_0)} \right]^{1/3}, \quad T = \frac{1}{\left[-\hat{r}_0^2\hat{h}_{,\hat{r}}(\hat{r}_0) \right]^{2/3}}. \quad (18)$$

Alternatively, one can compute $\hat{M} = \int_0^{\hat{r}_0} \hat{\rho}(\hat{r}, t) 4\pi\hat{r}^2 d\hat{r}$ and determine the temperature by $T = \hat{M}^{-2/3}$ and the radius by $r_0 = T^{1/2}\hat{r}_0$. On the other hand, using equations (193) and (11), the energy writes

$$E = \frac{3}{2}T - 3T^{5/2} \int_0^{\hat{r}_0} \left(\sqrt{1 + \hat{\rho}} - 1 \right)^2 4\pi\hat{r}^2 d\hat{r}. \quad (19)$$

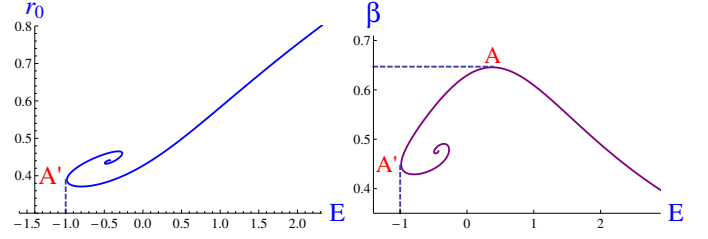


Fig. 1. Series of equilibria: Left: Radius versus energy $r_0(E)$; Right: inverse temperature versus energy $\beta(E)$. The curves are obtained by increasing the parameter \hat{h}_0 in the range $[0.5; 20]$ (smaller values of \hat{h}_0 are not represented as they correspond to the right parts of the curves which evolve monotonically).

We can also compute the energy at equilibrium from the relation (see Appendix A.2):

$$E = \frac{3}{2}T - \frac{1}{2r_0} + \frac{1}{2}T^{5/2} \int_0^{\hat{r}_0} \hat{h}_{,\hat{r}} \hat{M} d\hat{r}, \quad (20)$$

where we have used equations (5), (183), an integration by parts, and $\hat{\Phi} = -\hat{h} + C$ with $C = -1/(T^{3/2}\hat{r}_0) = -\hat{M}/\hat{r}_0$.

Varying \hat{h}_0 from 0 to $+\infty$ allows us to draw spiralling curves, such as $r_0(E)$ or $\beta(E)$, depicting the steady states. These curves (series of equilibria) are drawn in Figure 1. At high energies (and high temperatures), the star is stable since it reduces to a pure polytrope of index $\gamma = 2$ larger than $\gamma_c = 4/3$ [17]. Using Poincaré's bifurcation theory [19] (see [20,9] for an application of this theory in the case of self-gravitating systems), one can show that the series of equilibria remains stable in the microcanonical ensemble until the first turning point of energy (corresponding to $0 \leq \hat{h}_0 < \hat{h}_0^{(c)}$), and that it becomes unstable afterward (corresponding to $\hat{h}_0 > \hat{h}_0^{(c)}$). More precisely, a new mode of stability is lost at each turning point of energy. We focus here on the critical point A' where the first instability occurs as E decreases (\hat{h}_0 increases). It corresponds to a minimum of the energy, characterized by the following parameter values $\hat{h}_0^{(c)} = 6.50655$, $\hat{r}_0^{(c)} = 0.26074$, $\hat{\rho}_0^{(c)} = 2574$, $\hat{M}^{(c)} = 0.3012$, $\hat{P}_0^{(c)} = 2475$ or in non-hat scalings $\rho_0^{(c)} = 2574$, $r_0^{(c)} = 0.38897$, $P_0^{(c)} = 5508$, $E_c = -0.984142$ with $T_c = [\hat{M}^{(c)}]^{-2/3} = 2.22538$.

For these parameter values, the density profile is drawn in Figure 2-(a) where the arrow indicates the equilibrium radius (the radial distance where the solution crosses zero). Beyond this radius we set $\rho(r) = 0$, as in Paper I, whereas it leads to functions $\hat{\rho}(r)$, $\hat{M}(r)$, and $\hat{h}(r)$ with discontinuous slopes.

The mass enclosed inside a sphere of radius \hat{r} , $\hat{M}(\hat{r}) = \int_0^{\hat{r}} \hat{\rho}(r') 4\pi r'^2 dr'$, and the gravitational energy (also inside a sphere of radius \hat{r}) $W(\hat{r}) = -3T^{5/2} \int_0^{\hat{r}} (\sqrt{1 + \hat{\rho}} - 1)^2 4\pi r'^2 dr'$, are shown in Figures 2-(b) and 2-(c) respectively where the arrows display the radius at which the fluid motion is expected to separate (at critical) between opposite directions (inward and outward) at the saddle-center, as explained below.

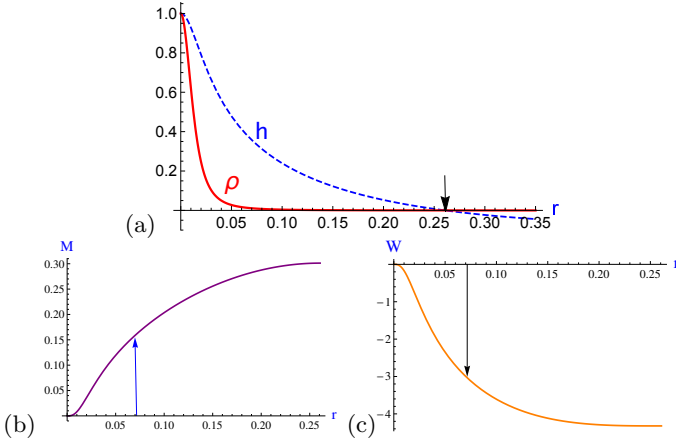


Fig. 2. (a) Density and enthalpy profiles $\hat{\rho}(\hat{r})/\hat{\rho}(0)$, $\hat{h}(\hat{r})/\hat{h}(0)$; (b) mass $\hat{M}(\hat{r})$ and (c) gravitational energy $W(\hat{r})$ at the microcanonical critical point A' (saddle-center). The arrow in (a) indicates the radius where the density and the enthalpy vanish, whereas the arrows in (b) and (c) display the radius where the velocity sign changes in the dynamical regime, see Subsection 2.3.3.

2.3 Saddle-center bifurcation in the microcanonical ensemble and linear stability analysis

We have seen in the previous section that the equation of hydrostatic equilibrium can have several solutions with the same energy E , but only one is stable. Close to A', two solutions (one stable and one unstable) merge. This defines a saddle-center bifurcation. Here, we investigate the structure of the critical mode.

2.3.1 Linearized Euler-Poisson system

The Euler-Poisson set of equations can be rewritten as

$$\frac{\partial \rho}{\partial t} + \nabla \cdot (\rho \mathbf{u}) = 0, \quad (21)$$

$$\frac{\partial}{\partial t}(\rho \mathbf{u}) + \nabla \cdot (\rho \mathbf{u} \otimes \mathbf{u}) = -\rho \nabla h - \rho \nabla \Phi, \quad (22)$$

$$\Delta \Phi = 4\pi \rho. \quad (23)$$

To determine the dynamical stability of a steady state of the Euler-Poisson system (21)-(23), we consider a small perturbation about that state and write $f(\mathbf{r}, t) = f(\mathbf{r}) + \delta f(\mathbf{r}, t)$ for $f = (\rho, \mathbf{u}, \Phi)$ with $\delta f(\mathbf{r}, t) \ll f(\mathbf{r})$. The linearized Euler-Poisson system writes

$$\frac{\partial \delta \rho}{\partial t} + \nabla \cdot (\rho \delta \mathbf{u}) = 0, \quad (24)$$

$$\frac{\partial}{\partial t}(\rho \delta \mathbf{u}) = -\rho \nabla \delta h - \rho \nabla \delta \Phi, \quad (25)$$

$$\Delta \delta \Phi = 4\pi \delta \rho. \quad (26)$$

These equations can be combined into a differential equation of the form

$$\frac{\partial^2 \delta \rho}{\partial t^2} = \nabla \cdot [\rho(\nabla \delta h + \nabla \delta \Phi)]. \quad (27)$$

Writing the time dependence of the perturbations as $\delta f(\mathbf{r}, t) \propto e^{\lambda t}$, we obtain the eigenvalue equation

$$\lambda^2 \delta \rho = \nabla \cdot [\rho(\nabla \delta h + \nabla \delta \Phi)], \quad (28)$$

which has to be solved in conjunction with the Poisson equation (26).

2.3.2 The point of marginal stability

We shall now investigate the behavior of the perturbations at the critical point. Our aim is to derive the radial profile of the marginal mode which results from the merging of the stable and unstable equilibrium states. In the case of the CEP model this amounts to solving an ODE with proper initial conditions (see Paper I), whereas the MEP model leads to an integro-differential equation, equations (43)-(45), that we may solve iteratively by changing one of the initial conditions, as explained below. The neutral mode ($\lambda = 0$) which signals the change of stability of the series of equilibria is the solution of the differential equation

$$\nabla \delta h^{(c)} + \nabla \delta \Phi^{(c)} = \mathbf{0}. \quad (29)$$

Therefore, at the critical point, we have

$$\delta h^{(c)}(\mathbf{r}) = -\delta \Phi^{(c)}(\mathbf{r}). \quad (30)$$

The constant of integration has been set equal to zero by assuming that the radius does not change at first order (see below). From this relation, and using Newton's law (181) in perturbed form, we obtain

$$\delta h_{,r}^{(c)} = -\delta \Phi_{,r}^{(c)} = \frac{\delta M^{(c)}(r)}{r^2}. \quad (31)$$

Taking the divergence of equation (29) and using Poisson's equation (26), we get

$$\Delta \delta h^{(c)} + 4\pi \delta \rho^{(c)} = 0. \quad (32)$$

The enthalpy h and the density ρ are linked by the relation

$$\rho(h, T) = 4 \left(e^{\frac{h}{T}} - e^{\frac{h}{2T}} \right). \quad (33)$$

The first order density deviation is given by

$$\delta \rho = \rho_{,h} \delta h + \rho_{,T} \delta T, \quad (34)$$

where

$$\rho_{,h} = \frac{4}{T} \left(e^{h/T} - \frac{1}{2} e^{h/2T} \right) \quad (35)$$

and

$$\rho_{,T} = -\frac{4h}{T^2} \left(e^{h/T} - \frac{1}{2} e^{h/2T} \right) \quad (36)$$

stand for the partial derivatives of $\rho(h, T)$ with respect to h and T , respectively. We have

$$\rho_{,T} = -\frac{h}{T}\rho_{,h}. \quad (37)$$

We also note that

$$\delta\rho(r_0) = \frac{2}{T}\delta h(r_0) \quad (38)$$

since $h(r_0) = 0$.

Substituting these relations into equation (32), we obtain

$$\Delta\delta h^{(c)} + 4\pi\rho_{,h}^{(c)}\delta h^{(c)} - 4\pi\frac{h^{(c)}}{T_c}\rho_{,h}^{(c)}\delta T^{(c)} = 0. \quad (39)$$

On the other hand, the energetic constraint (5) writes at first order

$$0 = \frac{3}{2}\delta T + \int \Phi\delta\rho\,dr. \quad (40)$$

Substituting equations (34)-(37) into equation (40), we get

$$\delta T = -\frac{\int \Phi\rho_{,h}\delta h\,dr}{\frac{3}{2} - \frac{1}{T}\int \Phi h\rho_{,h}\,dr}. \quad (41)$$

Finally, combining equations (39) and (41), we obtain the integral equation

$$\Delta\delta h^{(c)} + 4\pi\rho_{,h}^{(c)}\delta h^{(c)} + \frac{h^{(c)}}{T_c}\rho_{,h}^{(c)}\frac{4\pi\int \Phi^{(c)}\rho_{,h}^{(c)}\delta h^{(c)}\,dr}{\frac{3}{2} - \frac{1}{T_c}\int \Phi^{(c)}h^{(c)}\rho_{,h}^{(c)}\,dr} = 0, \quad (42)$$

which is the MEP version of the ordinary differential equation (25) of Paper I obtained for the CEP model free of the energetic constraint.

We now introduce the scaled variables of Section 2.2. Furthermore, we note $\hat{j} = \delta\hat{h}^{(c)}$ and $\hat{r}_c = \hat{r}_0^{(c)}$. From now on, we remove the “hats” to simplify the expressions. The integral equation (42) becomes

$$\Delta j + 4\pi\rho_{,h}^{(c)}j - 4\pi h^{(c)}\rho_{,h}^{(c)}\int_0^{r_c} j(r)f(r)\,dr = 0, \quad (43)$$

where

$$f(r) = -\frac{4\pi}{D}\rho_{,h}^{(c)}\Phi^{(c)}r^2 \quad (44)$$

and

$$D = \frac{3}{2T_c^{3/2}} - \int_0^{r_c} \Phi^{(c)}(r)h^{(c)}(r)\rho_{,h}^{(c)}4\pi r^2\,dr. \quad (45)$$

This equation has to be solved with the boundary condition $j_{,r}(r_c) = 0$ (see Appendix B) plus another condition, for example the value of $j(0)$. Because of the linearity of the integro-differential equation with respect to $j(r)$ we can set $\int_0^{r_c} j(r)f(r)\,dr = 1$, and vary $j(0)$ until the resulting solution satisfies this relation. We find that this occurs for $j(0) = 20.3$. The solution $j(r)$ is drawn in Figure 3, red curve. Finally, we note that the perturbed temperature at the critical point is given by

$$\mathcal{T} \equiv \frac{\delta T^{(c)}}{T_c} = \int_0^{r_c} j(r)f(r)\,dr = 1. \quad (46)$$

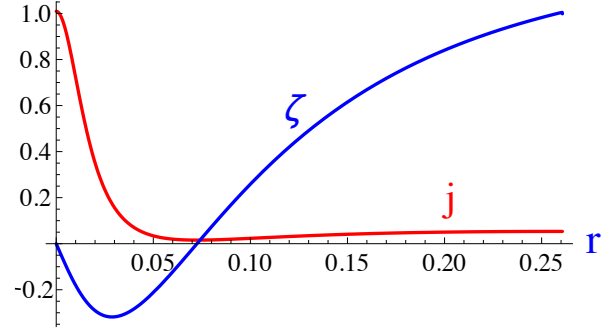


Fig. 3. Neutral mode $j(r)$ (red curve), positive everywhere, and function $\zeta(r)$ (blue curve) defined in Section 3.5, solution of equation (110).

2.3.3 The inward/outward motion

The radial profiles of mass, velocity and density deviations write as $\delta M^{(c)}(r) = -r^2 j_{,r}(r)$, $S^{(c)}(r) = j_{,r}(r)/4\pi\rho^{(c)}(r)$, and $\delta\rho^{(c)}(r) = \delta M_{,r}^{(c)}/4\pi r^2$, respectively (see Appendix B). The solution of equation (43) leads to the radial profiles shown in Figure 4. In Figure 4-(a), the insert is an enlargement of the lower part of the density deviation normalized by $\rho^{(c)}(r)$. It displays a small intermediate region of negative amplitude where the density of mass slightly decreases with respect to its equilibrium value. Figure 4-(b) clearly displays a simultaneous inward and outward motion of the fluid, the sign of the velocity profile $S^{(c)}$, or of the mass $\delta M^{(c)}$, changing at a radius about 28% of the star radius. When this value is reported on the curves of Figures 2-(b) and 2-(c) giving the mass $M(r)$ and the gravitational energy $W(r)$, they show that about 50% of the mass is expected to be expelled at the beginning of the supernova process, whereas the other half of the total mass begins to move inward. Concerning the gravitational energy, about 3/4 of it is concentrated in the inward-directed core, as indicated by the arrow in Figure 2-(c).

The inward/outward motion is illustrated by the radial displacement $S^{(c)}(r)$ shown in Figure 4-(b), red curve. We have to point out that, for the moment, the sign of the neutral mode is arbitrary since equation (43) defining the neutral mode profile $j(r)$ is linear. The sign of the radial profiles $S^{(c)}(r)$, $\delta M^{(c)}$ and $\delta\rho^{(c)}(r)$ represented in Figure 4 is actually derived from higher order terms of the weakly nonlinear analysis developed in the next Section. Figure 4-(b) shows that any particle located initially in the inner part of the star, $r < 0.073$, where the density is large (see Figure 2-(a)) should move inward, whereas any particle located in the outer shell should move outward. In the insert of Figure 4-(a) we show the ratio $\delta\rho^{(c)}/\rho$ which displays the two nodes behavior of the density deviation. It illustrates the formation of a mass close to the center plus a halo further away, and a decrease of density in between. In summary, we expect the formation of a sort of explosive halo together with a collapse of the inner part (core) from the first order variations at criticality. This important point has to be confirmed by the higher order

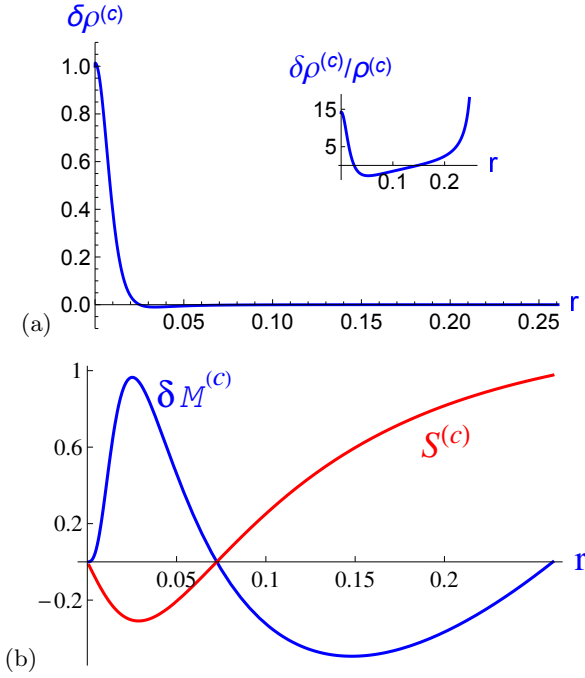


Fig. 4. Radial profiles of the first order deviations at the microcanonical critical point: (a) density $\delta\rho^{(c)}(r)$ (in the insert, the ratio $\delta\rho^{(c)}/\rho^{(c)}$ displays the two nodes behavior of the density deviation); (b) mass $\delta M^{(c)}(r)$ and velocity (or displacement) $S^{(c)}(r)$.

terms of the weakly nonlinear analysis, as done in next Section.

3 Dynamics close to the saddle-center bifurcation: derivation of the Painlevé I equation

In this Section, we focus on the first stage of the motion, when the system approaches the critical point A' in Figure 1 by decreasing the energy $E(t)$, following the stable portion of the series of equilibria. Note that here and in Paper I we call this weakly nonlinear stage “the Painlevé regime”, and we call the analysis of the saddle-center bifurcation “the Painlevé analysis”, whereas in the work of Painlevé no connection is made with bifurcation theory². In this Painlevé regime, because the velocity field has a small amplitude at the beginning of the motion, we assume that the advection term can be neglected in the Euler equation, an hypothesis that is justified during a time interval t_0 by using the same arguments as in Section 4.1 of Paper I (the time interval t_0 can be defined in terms of the coefficients appearing in the normal form of the Euler equations close to the saddle-center, i.e., the Painlevé I equation). In this Section, we use the same procedure and

notations as in Section 4 of Paper I, but this Section is self-contained.

3.1 Simplification of the hydrodynamic equations

Neglecting the advection term in the Euler equation (22) we obtain

$$\frac{\partial}{\partial t}(\rho \mathbf{u}) = -\nabla P - \rho \nabla \Phi. \quad (47)$$

This equation can be combined with the equation of continuity (21) into a single equation for the density

$$\frac{\partial^2 \rho}{\partial t^2} = \nabla \cdot (\nabla P + \rho \nabla \Phi), \quad (48)$$

where Φ is given by the Poisson equation (23). The energetic constraint writes

$$E = \frac{3}{2}T(t) + \frac{1}{2} \int \rho \Phi d\mathbf{r}. \quad (49)$$

These equations are valid during a time interval of order t_0 before the collapse time (see Paper I).

3.2 The equation for the mass profile

For a spherically symmetric evolution, using Newton's law (181), we obtain the following partial differential equation for the integrated density

$$\frac{\partial^2 M(r, t)}{\partial t^2} = 4\pi r^2 P_{,r} + \frac{1}{r^2} M_{,r} M. \quad (50)$$

The energetic constraint writes

$$E = \frac{3}{2}T(t) + \frac{1}{2} \int_0^{R(t)} \Phi M_{,r} dr. \quad (51)$$

In equation (50), the term $P_{,r} = P_{,\rho}(\rho) \rho_{,r}$ has to be expressed as a function of $\rho(r, t) = M_{,r}/(4\pi r^2)$ and $\rho_{,r}(r, t) = (M_{,r^2} - 2M_{,r}/r)/(4\pi r^2)$. For the equation of state

$$P(\rho) = T(t) \left(\sqrt{1 + \rho} - 1 \right)^2, \quad (52)$$

we get

$$P_{,\rho}(\rho) = T(t) \left(1 - \frac{1}{\sqrt{1 + \rho}} \right). \quad (53)$$

Introducing this expression into equation (50), the dynamical equation for $M(r, t)$ writes

$$\frac{\partial^2 M(r, t)}{\partial t^2} = T(t) \mathcal{L}(M) g(M_{,r}) + \frac{1}{r^2} M_{,r} M \quad (54)$$

with

$$\begin{cases} \mathcal{L}(M) = M_{,r^2} - \frac{2}{r} M_{,r} \\ g(M_{,r}) = 1 - \frac{1}{\sqrt{1 + \frac{1}{4\pi r^2} M_{,r}}} \end{cases} \quad (55)$$

² Painlevé found these equations when searching solutions having peculiar properties related to the position of their complex singularities

The boundary conditions to be satisfied are

$$\begin{cases} M(0, t) = 0 \\ M(R(t), t) = 1 = 4\pi \int_0^{R(t)} dr' r'^2 \rho(r', t). \end{cases} \quad (56)$$

In the latter relation, the radius of the star $R(t)$ depends on time. However, this dependence will be neglected in this Painlevé analysis because it can be shown that it plays no role up to order two (with respect to the small parameter ϵ which characterizes the slow time dependence of E), the order considered below. Therefore, we take $R(t) \simeq r_0$.

3.3 Equilibrium state and neutral mode for the mass profile

The steady solution of equation (54) is determined by the partial differential equation

$$T\mathcal{L}(M)g(M_{,r}) + \frac{1}{r^2}M_{,r}M = 0 \quad (57)$$

with the energetic constraint

$$E = \frac{3}{2}T + \frac{1}{2} \int_0^{r_0} \Phi M_{,r} dr. \quad (58)$$

We now consider a small perturbation about a steady state and write $M(r, t) = M(r) + \delta M(r, t)$ with $\delta M(r, t) \ll M(r)$. Linearizing equation (54) about this steady state and writing the time dependence of the perturbation as $\delta M(r, t) \propto e^{\lambda t}$, we obtain the eigenvalue equation

$$\begin{aligned} \lambda^2 \delta M = T [\mathcal{L}(\delta M)g(M_{,r}) + \mathcal{L}(M)g'(M_{,r})\delta M_{,r}] \\ + \delta T \mathcal{L}(M)g(M_{,r}) + \frac{1}{r^2}(M\delta M)_{,r} \end{aligned} \quad (59)$$

with the energy constraint

$$\frac{3}{2}\delta T + \int_0^{r_0} \Phi \delta M_{,r} dr = 0. \quad (60)$$

The neutral mode, corresponding to $\lambda = 0$, is determined by the differential equation

$$\begin{aligned} T [\mathcal{L}(\delta M)g(M_{,r}) + \mathcal{L}(M)g'(M_{,r})\delta M_{,r}] \\ + \delta T \mathcal{L}(M)g(M_{,r}) + \frac{1}{r^2}(M\delta M)_{,r} = 0. \end{aligned} \quad (61)$$

3.4 Scaled variables

To study the dynamics close to the critical point A' , we introduce the scaled variables $\hat{r} = r/\sqrt{T_c}$, $\hat{t} = t$, $\hat{M} = M/T_c^{3/2}$, $\hat{h} = h/T_c$, $\hat{\Phi} = \Phi/T_c$, $\hat{\rho} = \rho$, $\hat{E} = E/T_c$, and $\hat{T} = T/T_c$. At the critical point, we have $\hat{T} = 1$ and all the other variables coincide with those introduced in Section 2.2. In the following, we drop the “hats” to simplify the notations. With this rescaling, we obtain

$$\frac{\partial^2 M(r, t)}{\partial t^2} = T(t)\mathcal{L}(M)g(M_{,r}) + \frac{1}{r^2}M_{,r}M \quad (62)$$

with the boundary conditions

$$\begin{cases} M(0, t) = 0 \\ M(r_c, t) = T_c^{-3/2} = 4\pi \int_0^{r_c} dr' r'^2 \rho(r', t). \end{cases} \quad (63)$$

The energetic constraint writes

$$E = \frac{3}{2}T(t) + \frac{1}{2}T_c^{3/2} \int_0^{r_0} \Phi M_{,r} dr. \quad (64)$$

The steady solution of equation (62) at the critical point is determined by

$$\mathcal{L}(M^{(c)})g(M_{,r}^{(c)}) + \frac{1}{r^2}M_{,r}^{(c)}M^{(c)} = 0 \quad (65)$$

with the energetic constraint

$$E_c = \frac{3}{2} + \frac{1}{2}T_c^{3/2} \int_0^{r_c} \Phi^{(c)} M_{,r}^{(c)} dr. \quad (66)$$

Using Newton's law $\Phi_{,r} = M(r)/r^2$, and the equilibrium relation $\Phi_{,r} = -h_{,r}$, we can easily check that equation (65) is equivalent to equation (16). On the other hand, at the critical point, the marginal mode ($\lambda = 0$) is determined by the differential equation [see equation (61)]:

$$\begin{aligned} \mathcal{L}(\delta M^{(c)})g(M_{,r}^{(c)}) + \mathcal{L}(M^{(c)})g'(M_{,r}^{(c)})\delta M_{,r}^{(c)} \\ + \delta T \mathcal{L}(M^{(c)})g(M_{,r}^{(c)}) + \frac{1}{r^2}(M^{(c)}\delta M^{(c)})_{,r} = 0 \end{aligned} \quad (67)$$

with the energy constraint

$$\frac{3}{2}\delta T + T_c^{3/2} \int_0^{r_c} \Phi^{(c)} \delta M_{,r}^{(c)} dr = 0. \quad (68)$$

Using Newton's law in perturbed form $\delta\Phi_{,r} = \delta M(r)/r^2$, and the relation $\delta\Phi_{,r}^{(c)} = -\delta h_{,r}^{(c)}$ satisfied at the neutral point (see Section 2.3.2), we can check that equation (67) is equivalent to equation (43). This implies that the neutral mass profile is given by

$$\delta M^{(c)}(r) = -r^2 j_{,r}, \quad (69)$$

where $j(r)$ has been determined in Section 2.3.2.

3.5 Normal form close to the saddle-center bifurcation

The derivation of the normal form of the hydrodynamic equations close to the saddle-center bifurcation proceeds by expanding the different quantities close to their equilibrium value at critical energy E_c in series of a small parameter ϵ which characterizes a slow variation of the energy with respect to its value at the saddle-center, supposed to evolve as $E(t) = E_c - \gamma't$, with γ' small. We set

$$E = E_c - \epsilon^2 E^{(2)}, \quad (70)$$

which amounts to defining $\epsilon^2 E^{(2)} = \gamma't$, and rescaling the time as $t = t'/\epsilon^{1/2}$. Equation (62) is then rewritten as

$$\epsilon \frac{\partial^2 M}{\partial t'^2} = T(t')\mathcal{L}(M)g(M_{,r}) + \frac{1}{r^2}M_{,r}M. \quad (71)$$

The radial distribution of mass (or radial profile) is expanded as

$$M(r, t') = M^{(c)}(r) + \epsilon M^{(1)}(r, t') + \epsilon^2 M^{(2)}(r, t') + \dots \quad (72)$$

where $M^{(c)}(r)$ is the equilibrium profile at $E = E_c$ (see above) drawn in Figure 2-(b). The expansion of the energy is given in equation (70) and the expansion of the temperature reads

$$T(t') = 1 + \epsilon T^{(1)}(t') + \epsilon^2 T^{(2)}(t') + \dots \quad (73)$$

We now substitute the expansion (72) into equation (71) and consider each order.

3.5.1 Leading order

At leading order, we get the equilibrium relation

$$\mathcal{L}^{(c)} g^{(c)} + \frac{1}{r^2} M_{,r}^{(c)} M^{(c)} = 0 \quad (74)$$

which has to satisfy the boundary conditions

$$M^{(c)}(0) = M_{,r}^{(c)}(0) = 0, \quad M^{(c)}(r_c) = M = T_c^{-3/2}. \quad (75)$$

The energy constraint writes

$$E_c = \frac{3}{2} + \frac{1}{2} T_c^{3/2} \int_0^{r_c} \Phi^{(c)} M_{,r}^{(c)} dr. \quad (76)$$

The mass profile at the critical point is drawn in Figure 2-(b).

3.5.2 First order

To order 1 with respect to ϵ , we have

$$T^{(1)} \mathcal{L}^{(c)} g^{(c)} + \mathcal{L}^{(1)} g^{(c)} + \mathcal{L}^{(c)} g^{(1)} + \frac{1}{r^2} (M^{(1)} M^{(c)})_{,r} = 0, \quad (77)$$

with the energy constraint giving

$$T^{(1)} = -\frac{2}{3} T_c^{3/2} \int_0^{r_c} \Phi^{(c)}(r) M_{,r}^{(1)} dr. \quad (78)$$

Because equation (77) is linear, its solution is of the form

$$M^{(1)}(r, t') = A^{(1)}(t') F(r), \quad (79)$$

$$T^{(1)}(t') = A^{(1)}(t') \mathcal{T}, \quad (80)$$

$$h^{(1)}(r, t') = A^{(1)}(t') j(r), \quad (81)$$

$$S^{(1)}(r, t') = A^{(1)}(t') S^{(c)}(r), \quad (82)$$

$$u^{(1)}(r, t') = \epsilon^{1/2} \dot{A}^{(1)}(t') S^{(c)}(r). \quad (83)$$

This corresponds to the neutral mode multiplied by $A^{(1)}(t')$. In the foregoing equations $F(r) = \delta M^{(c)}(r)$, $\mathcal{T} = \delta T^{(c)}$, $j(r) = \delta h^{(c)}(r)$ and the dot in equation (83) stands for the time derivative. The neutral mode profiles (enthalpy, density, mass, and velocity) are plotted in Figures 3 and 4. The function $F(r) = \delta M^{(c)}(r)$ was actually derived from the solution $j(r)$ of equation (43) thanks to the relation

$$F(r) = -r^2 j_{,r}. \quad (84)$$

3.5.3 Second order

To order 2, equation (71) gives

$$\frac{\partial^2 M^{(1)}}{\partial t'^2} = T^{(2)} \mathcal{L}^{(c)} g^{(c)} + T^{(1)} (\mathcal{L}^{(1)} g^{(c)} + \mathcal{L}^{(c)} g^{(1)}) + \mathcal{F}^{(2)}, \quad (85)$$

where

$$\mathcal{F}^{(2)} = \mathcal{L}^{(2)} g^{(c)} + \mathcal{L}^{(1)} g^{(1)} + \mathcal{L}^{(c)} g^{(2)} + \mathcal{F}_1^{(2)} \quad (86)$$

and

$$\mathcal{F}_1^{(2)} = \frac{1}{r^2} [(M^{(2)} M^{(c)})_{,r} + M^{(1)} M_{,r}^{(1)}] \quad (87)$$

with

$$\mathcal{L}^{(c)} = \mathcal{L}(M^{(c)}), \quad \mathcal{L}^{(n)} = \mathcal{L}(M^{(n)}), \quad (88)$$

$$g^{(1)} = g'^{(c)} M_{,r}^{(1)}, \quad g^{(2)} = \frac{1}{2} g''^{(c)} (M_{,r}^{(1)})^2 + g'^{(c)} M_{,r}^{(2)}, \quad (89)$$

$$g^{(c)} = g(M_{,r}^{(c)}), \quad g'^{(c)} = \left(\frac{dg}{dM_{,r}} \right)^{(c)}, \quad g''^{(c)} = \left(\frac{d^2 g}{dM_{,r}^2} \right)^{(c)}. \quad (90)$$

The r -dependent quantities can be written in terms of the equilibrium density function $\rho^{(c)}(r)$ as

$$\begin{cases} \mathcal{L}^{(c)} = 4\pi r^2 \rho_{,r}^{(c)}, \\ g^{(c)} = 1 - \frac{1}{\sqrt{1+\rho^{(c)}}}, \\ g'^{(c)} = \frac{1}{8\pi r^2 (1+\rho^{(c)})^{3/2}}, \\ g''^{(c)} = -\frac{3}{4(4\pi r^2)^2 (1+\rho^{(c)})^{5/2}}. \end{cases} \quad (91)$$

The boundary conditions are

$$\begin{cases} M^{(n)}(0, t') = 0, & M_{,r}^{(n)}(0, t') = 0, \\ M^{(n)}(r_c, t') = 0. \end{cases} \quad (92)$$

The energetic constraint writes

$$\begin{aligned} -E^{(2)} &= \frac{3}{2} T^{(2)} + \frac{1}{2} T_c^{3/2} \int_0^{r_c} \Phi^{(1)} M_{,r}^{(1)} dr \\ &\quad + T_c^{3/2} \int_0^{r_c} \Phi^{(c)} M_{,r}^{(2)} dr. \end{aligned} \quad (93)$$

This determines $T^{(2)}$. In terms of $M^{(n)}$ the resonant and non-resonant parts of the second order temperature deviation $T^{(2)} = T_{\text{res.}}^{(2)} + T_{\text{n.res.}}^{(2)}$ are given by the relations

$$\begin{aligned} T_{\text{res.}}^{(2)} &= -\frac{2}{3} T_c^{3/2} \int_0^{r_c} \Phi^{(c)} M_{,r}^{(2)} dr \\ &= -\frac{2}{3} T_c^{3/2} \int_0^{r_c} h_{,r}^{(c)} M^{(2)} dr \end{aligned} \quad (94)$$

and

$$\begin{aligned} T_{\text{n.res.}}^{(2)} &= -\frac{1}{3} T_c^{3/2} \int_0^{r_c} \Phi^{(1)} M_{,r}^{(1)} dr - \frac{2}{3} E^{(2)} \\ &= -\frac{1}{3} T_c^{3/2} \int_0^{r_c} h_{,r}^{(1)} M^{(1)} dr - \frac{2}{3} E^{(2)}. \end{aligned} \quad (95)$$

Using equations (79) and (81), we get

$$T_{\text{n.res.}}^{(2)} = -\frac{1}{3}T_c^{3/2}[A^{(1)}]^2 \int_0^{r_c} j_{,r}(r)F(r) dr - \frac{2}{3}E^{(2)}. \quad (96)$$

After splitting the resonant and non-resonant terms in equation (85), we obtain

$$F(r)\ddot{A}^{(1)}(t') = T_{\text{n.res.}}^{(2)}\mathcal{L}^{(c)}g^{(c)} + \mathcal{K}(F)[A^{(1)}]^2 + \mathcal{C}(M^{(2)}), \quad (97)$$

where the non-resonant contribution to the quadratic term is

$$\begin{aligned} \mathcal{K}(F) = & \frac{1}{r^2}FF_{,r} + \frac{1}{2}\mathcal{L}^{(c)}g''^{(c)}F_{,r}^2 + g'^{(c)}\mathcal{L}(F)F_{,r} \\ & + \mathcal{T}\left(\mathcal{L}(F)g^{(c)} + \mathcal{L}^{(c)}g'^{(c)}F_{,r}\right), \end{aligned} \quad (98)$$

whereas the resonant term is

$$\begin{aligned} \mathcal{C}(M^{(2)}) = & \mathcal{L}^{(2)}g^{(c)} + \frac{1}{r^2}(M^{(2)}M^{(c)})_{,r} \\ & + \mathcal{L}^{(c)}g'^{(c)}M_{,r}^{(2)} + T_{\text{res}}^{(2)}\mathcal{L}^{(c)}g^{(c)}. \end{aligned} \quad (99)$$

Substituting equation (96) into equation (97), introducing the slow decrease of the energy versus time, $E^{(2)} \sim \gamma't/\epsilon^2$, and making the rescaling $A = \epsilon A^{(1)}$ to eliminate ϵ (we note that $A(t)$ is the true amplitude of the mass profile $M^{(1)}(r, t)$), we get

$$\begin{aligned} F(r)\ddot{A} = & -\frac{2}{3}\gamma't\mathcal{L}^{(c)}g^{(c)} + \epsilon^2\mathcal{C}(M^{(2)}) \\ & + \left[\mathcal{K}(F) - \frac{1}{3}T_c^{3/2}\mathcal{L}^{(c)}g^{(c)} \int_0^{r_c} j_{,r}(r)F(r) dr\right] A^2. \end{aligned} \quad (100)$$

3.5.4 Solvability condition

To write the dynamical equation for $A(t)$ in a normal form, we multiply equation (100) by a function $\zeta(r)$ and integrate over r for $0 < r < r_c$. We are going to derive the function $\zeta(r)$ so that the term $\mathcal{C}(M^{(2)})$ disappears after integration. By definition, the function ζ must satisfy, for any function $M^{(2)}(r)$, the integral relation

$$\int_0^{r_c} \mathcal{C}(M^{(2)})(r)\zeta(r) dr = 0. \quad (101)$$

Let us expand \mathcal{C} as

$$\mathcal{C}(M^{(2)}) = g^{(c)}M_{,r^2}^{(2)} + bM_{,r}^{(2)} + cM^{(2)} + \mathcal{I}[M^{(2)}], \quad (102)$$

where

$$\mathcal{I}[M^{(2)}] = \delta(r) \int_0^{r_c} h_{,r}^{(c)} M^{(2)} dr \quad (103)$$

with

$$\delta(r) = -\frac{2}{3}T_c^{3/2}\mathcal{L}^{(c)}(r)g^{(c)}(r). \quad (104)$$

We have also introduced $b(r) = -2g^{(c)}/r + M^{(c)}/r^2 + \mathcal{L}^{(c)}g'^{(c)}$ and $c(r) = M_{,r}^{(c)}/r^2$. In terms of the equilibrium

values of the density and potential functions at the saddle-center, we have

$$\begin{cases} g^{(c)}(r) = 1 - \frac{1}{\sqrt{1+\rho^{(c)}}}, \\ b(r) = -\frac{2g^{(c)}}{r} - h_{,r}^{(c)} + \frac{\rho_{,r}^{(c)}}{2(1+\rho^{(c)})^{3/2}}, \\ c(r) = 4\pi\rho^{(c)}. \end{cases} \quad (105)$$

Integrating the first three terms of $\mathcal{C}(M^{(2)})(r)$ in equation (101) by parts, using $M^{(2)}(r) = 0$ on the boundaries $r = 0$ and $r = r_c$, and using $M_{,r}^{(2)}(0) = 0$ and $g^{(c)}(r_c) = 0$, gives

$$\begin{aligned} & \int_0^{r_c} dr M^{(2)}\mathcal{D}[\zeta] \\ & + \int_0^{r_c} dr \zeta(r)\delta(r) \int_0^{r_c} dr M^{(2)}(r)h_{,r}^{(c)}(r) = 0, \end{aligned} \quad (106)$$

where the action of the differential operator $\mathcal{D}[\cdot]$ on a function $\zeta(r)$ is such that

$$\mathcal{D}[\zeta] = (g^{(c)}\zeta)_{,r^2} - (b\zeta)_{,r} + c\zeta. \quad (107)$$

It can be written equivalently as

$$\mathcal{D}[\zeta] = g^{(c)}(r)\zeta_{,r^2} + a_1(r)\zeta_{,r} + a_0(r)\zeta, \quad (108)$$

where the coefficients

$$\begin{cases} a_1(r) = 2g_{,r}^{(c)} - b(r), \\ a_0(r) = c(r) + g_{,r^2}^{(c)}(r) - b_{,r}(r), \end{cases} \quad (109)$$

can be expressed in terms of the radial density by using equations (91) and (105). The function ζ is the solution of the integro-differential equation

$$\mathcal{D}[\zeta] + h_{,r}^{(c)}(r) \int_0^{r_c} \zeta(r)\delta(r) dr = 0. \quad (110)$$

The solution $\zeta(r)$ is drawn in Figure 3, blue curve. This solution is obtained by solving the integro-differential equation (110) with two initial conditions. Close to the center, it can be shown that the solution of equation (110) writes $\zeta(r) = z_1r + z_3r^3 + \dots$. Therefore we set $\zeta(0) = 0$ and $\zeta'(0) = z_1$, an a priori unknown parameter proportional to $G \equiv \int_0^{r_c} \zeta(r)\delta(r) dr$ which may be taken as unity since the integro-differential equation is linear with respect to ζ . The value z_1 of the slope of $\zeta(r)$ at the center is determined numerically by increasing z_1 step by step. At step n , for a given $z_1^{(n)}$, we solve the ordinary differential equation

$$\mathcal{D}[\zeta^{(n)}] + h_{,r}^{(c)}(r) = 0, \quad (111)$$

calculate the value of $\int_0^{r_c} \zeta^{(n)}(r)\delta(r) dr$, and increase the slope z_1 until we obtain the expected result $\int_0^{r_c} \zeta(r)\delta(r) dr = 1$.

3.5.5 Painlevé I equation

Now that we have obtained the function $\zeta(r)$ satisfying the integral relation (101), we find that equation (100)

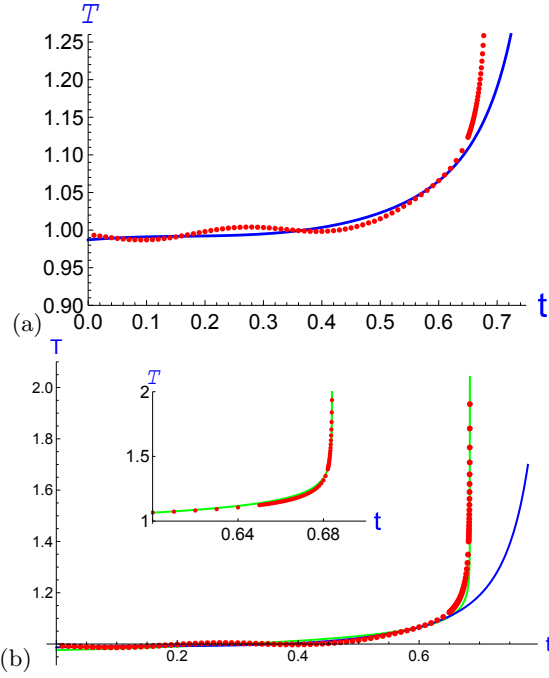


Fig. 5. Evolution of the temperature (a) in the Painlevé regime, $0 \lesssim t \lesssim 0.6$, (b) in the whole time interval before collapse, $0 \lesssim t \lesssim 0.684$. The numerical solution (dots) of the MEP model with the energetic constraint $E = E_c - \gamma'(t - t_0)$, where $\gamma' = 0.1$, is compared in (a) with the solution $A(t)$ of the Painlevé I equation (112) with the initial condition $A(t_0) = -0.008$ and $\dot{A}(t_0) = 0.01$, where $t_0 = 0.18$. In (b) we add the self-similar solution $T(t) \sim (t - t_*)^{a(k)}$ of Section 4.1 where $k = 8$ ($a = -1/24$) in the green portion of the principal curve, and $k = 8.4$ ($a = -0.074$) in the insert.

multiplied by $\zeta(r)$ and integrated over r for $0 < r < r_c$ takes the form of the Painlevé I equation

$$\ddot{A}(t) = \tilde{\gamma}t + KA^2. \quad (112)$$

The first coefficient in equation (112) is given explicitly as a function of the parameters at the critical point by the expression

$$\tilde{\gamma} = -\frac{2}{3}\gamma' \frac{\int_0^{r_c} \mathcal{L}^{(c)}(r)g^{(c)}(r)\zeta(r)dr}{\int_0^{r_c} F(r)\zeta(r)dr} \quad (113)$$

which is found to be equal to $\tilde{\gamma} = 46.63... \gamma'$. Moreover, the second coefficient in equation (112) is given by

$$K = \frac{\int_0^{r_c} \mathcal{G}(r)\zeta(r)dr}{\int_0^{r_c} F(r)\zeta(r)dr} \quad (114)$$

with

$$\begin{aligned} \mathcal{G}(r) = & \mathcal{L}^{(c)} F_{,r} \left(\frac{1}{2} g^{(c)} F_{,r} + \mathcal{T} g^{(c)} \right) \\ & + \left(g^{(c)} F_{,r} + \mathcal{T} g^{(c)} \right) \left(F_{,r^2} - \frac{2}{r} F_{,r} \right) + \frac{1}{r^2} F F_{,r} \\ & + \frac{1}{3} \mathcal{L}^{(c)} g^{(c)} T_c^{3/2} \int_0^{r_c} j(r) F_{,r}(r) dr. \end{aligned} \quad (115)$$

It is found to have the numerical value $K = 1055.98...$

As noted in Section 2.3.3, an important point to make clear is the sign of the neutral mode which was unknown at first order. With the choice we made in the previous Section, we obtain at second order two positive coefficients $\tilde{\gamma}$ and K in the Painlevé equation (112). This result confirms that we made the good choice at first order, because it leads to the acceleration of the velocity field initially chosen. A change of sign of the neutral mode amounts to changing A into $-A$ in the Painlevé equation (112), or to changing the sign of the nonlinear coefficient K (this change of sign being formal because it is just a consequence of the sign chosen for the neutral mode). *In fine*, this imposes us to reverse $-A$ into A because we want to look at a growing perturbation. In summary, the weakly nonlinear analysis provides the time evolution of the perturbation *and* the sign of the growing mode. This is an intrinsic property of saddle-center bifurcations which is absent in the case of “classical” transitions from a linearly stable to a linearly unstable situation, where the unstable mode may have either positive or negative amplitude. Such a fair property of saddle-center bifurcations comes from the fact that the stable and unstable equilibrium states are merging at the critical point, so that no equilibrium state exists beyond that point.

We now compare the prediction of the weakly nonlinear analysis derived here with the solution of the full MEP model. The numerical solutions of the full MEP model were obtained using a variant of the CentPack Software [21, 22] by Balbas and Tadmor, with a spatial mesh of 3000 points and adaptative time increments. In Figure 5-(a), we plot in solid line the temperature $T(t) = \mathcal{T}A(t)$ resulting from the above Painlevé analysis and show in dotted line the temperature calculated with the full numerical MEP model for the early stage of the explosion-implosion process. In the numerical study of the MEP model, our aim was to take as initial condition the equilibrium state at the critical energy E_c defined theoretically in Section 2.2, and let the energy slowly decrease. However, the numerical value of the equilibrium state in the MEP solution is not exactly the one predicted by the theory (point A' in Figure 1) because of finite mesh effects, as already observed in the canonical case (Paper I). Here, the density in the core is about two orders of magnitude larger than in Paper I, causing rapid fluctuations of the MEP solution around an average value. These fluctuations are clearly visible on the temperature $T(t)$ of Figure 5-(a) which displays a few oscillations before increasing strongly. Such rapid oscillations are not observed in solving Painlevé's equation: with off-equilibrium initial conditions close to the critical point, we would get oscillations with a long period as described in Paper I (see Figure 2 and equation (10)). The rapid oscillations observed here could be attributed to acoustic waves formed because of the stiffness of the density. They are characterized by a back and forth motion of matter in the star, as illustrated in Figure 6 which reports the deviations of mass and velocity in the whole star versus r at various times in the weakly nonlinear regime. Due to this back-and-forth motion, the

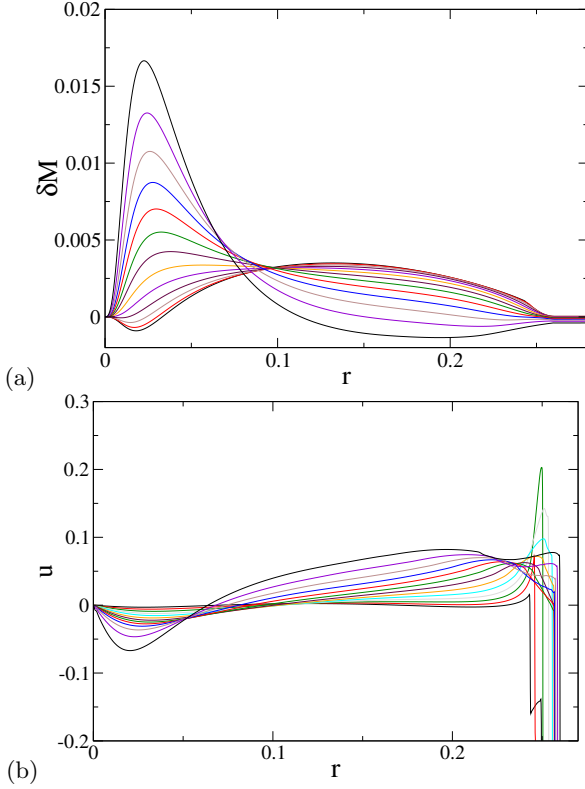


Fig. 6. Fluctuations of mass and velocity of the MEP model showing the back and forth motion concomitant with the oscillations of temperature $T(t)$ during the Painlevé regime. We also see that the velocity is negative in the core and positive in the halo. Therefore, these direct numerical simulations confirm the inward/outward motion of the star predicted by our linear or weakly nonlinear analysis close to the critical point. Furthermore, the numerical profiles $\delta M(r, t)$ and $\delta u(r, t)$ are in qualitative agreement with the radial profiles of the first order deviations at the microcanonical critical point plotted in Figure 4.

MEP profiles shown in this figure agree only qualitatively with the neutral mode profiles shown in Figure 4-(b). Note that the fluid mechanical equations we solve are without any damping term, so spurious time oscillations are easily generated in the numerics.

To compare the temperature of the MEP model with the weakly nonlinear analysis, we take as initial conditions of the Painlevé equation the ones of the MEP solution averaged over the oscillations at a given time $t_0 = 0.18$ which is chosen close to the point where $T(t) = T_c = 1$ (in normalized variables). The agreement between the MEP model and the weakly nonlinear analysis (see Figure 5-(a)) is very good until $t_s = 0.6$ which characterizes the end of the Painlevé regime where nonlinear terms of higher order come into play. After $t = t_s$, the two curves separate, the solution of the full equations increasing much more strongly than the weakly nonlinear one. The solution of the full equations has a self-similar behavior leading to a finite time singularity at $t_* \simeq 0.684$ illustrated by the green portion of the curve (see the next Section). The so-

lution of the Painlevé equation also displays a divergence but it occurs later (at $t_P \simeq 0.8$), in a regime where the Painlevé equation is not valid anymore (see below).

The duration of the Painlevé regime is expected to be a few times the precursor time (intermediate time scale) which stands between the short and long time scales, defined in Section 2 of Paper I, and given by the relation

$$t_0 = (\tilde{\gamma}K)^{-1/5}. \quad (116)$$

Introducing the numerical values of K and $\tilde{\gamma}$ in equation (116), we obtain $t_0 = 0.18$ which is about 1/3 the full Painlevé regime duration illustrated in Figure 5-a, as expected.

In the framework of Painlevé’s equation, the collapse time is given by the relation $t_P \simeq 3.4t_0$, or $t_P \simeq 0.4|T_c/T|^{1/5}$, where $\dot{T}/T_c = \gamma'$ (see Paper I). Numerically, this gives $t_P^{\text{approx}} = 0.63$. This approximate value agrees well with the exact Painlevé diverging time $t_P = 0.8$ when taking the origin at $t_0 = 0.18$. Note that this “Painlevé” collapse time is not reached by the solution of the MEP model which diverges before at $t_* \simeq 0.684$. On the other hand, we have shown in Paper I that the amplitude of the Painlevé solution (for example the temperature drawn in solid line) diverges close to t_P as

$$A(t) = \frac{0.0063}{(t_P - t)^2}, \quad (117)$$

a solution different from the MEP model solution as discussed in the next Section [see equation (123)].

4 The post-Painlevé regime before explosion (pre-collapse regime)

After the weakly nonlinear Painlevé regime, the full numerical MEP model displays a solution which ultimately diverges at t_* defined as the collapse time. This divergence occurs in the core domain whose radius shrinks to zero while the density and the velocity increase up to infinity there. Simultaneously, the temperature also diverges as shown in Figure 5-(b). In the halo, the outward velocities continue to grow, but more slowly than in the core, so that at the collapse time t_* the outward motion of matter is still at an early stage. The solution of the MEP model will be described separately in the two regions.

4.1 Core collapse

The increase of density and velocity close to the center of the star, which are well visible in linear scale in Figures 7-(a) and 9-(a), deserves to be specified. The numerical study displays a solution which becomes self-similar in the core after the Painlevé regime, with a singularity of the second kind in the sense of Zel’dovich [23]. This property was already found in the canonical case (Paper I) where the whole star collapses. In both cases, in the

collapsing domain, the values of the exponents characterizing the self-similar regime show that gravity dominates over pressure forces. However, direct numerical simulations show that the exponents of the MEP model are different from those of the CEP model. Recall that for the gravity-dominated case, using the notations of Paper I, the self-similar density is of the form

$$\rho(r, t) = (-t)^{-2} R(r(-t)^{-2/\alpha}), \quad (118)$$

and the self-similar velocity is of the form

$$u(r, t) = (-t)^{-1+\frac{2}{\alpha}} U(r(-t)^{-2/\alpha}), \quad (119)$$

where R and U are invariant profiles, $\xi = r(-t)^{-2/\alpha}$ is the scaled radial distance, and the exponent α is larger than two. We have taken the origin of time at the collapse time t_* . These self-similar solutions require that $R(\xi) \sim \xi^{-\alpha}$ and $U(\xi) \sim \xi^{-(\alpha/2-1)}$ for $\xi \rightarrow +\infty$ in order to have a steady profile at large distances, as necessary. The exponent α is not free; it is related to the behavior of the self-similar solution as $\xi \rightarrow 0$ [3]. More precisely, expanding R as $R = R_0 + R_2 \xi^2 + \dots + R_k \xi^k + \dots$ and U as $U = U_1 \xi + \dots + U_k \xi^{k+1} + \dots$, one finds

$$\alpha(k) = \frac{6k}{2k+3}, \quad (120)$$

where k is an even number because we consider solutions with spherical symmetry.

The behavior of the temperature

$$T(t) = \frac{2}{3}E - \frac{1}{3} \int \rho \Phi d\mathbf{r} - \frac{1}{3} \int \rho \mathbf{u}^2 d\mathbf{r}, \quad (121)$$

can be deduced from the above scalings in the core domain. This can be done if one neglects the contribution of the halo to the energy in equation (121), an assumption justified because the kinetic and gravitational energies are much smaller in the halo than in the core.³ In the core, the potential energy behaves as $W \sim \rho_c \Phi_c r_0^3$, where $\Phi_c \sim -\rho_c r_0^2$ according to Poisson's equation. Using $\rho_c \sim (-t)^{-2}$ and $r_0 \sim (-t)^{2/\alpha}$, we get

$$T \sim -W \sim (-t)^{10/\alpha-4} \sim (-t)^{\frac{15-2k}{3k}} \quad (122)$$

which diverges for α larger than $5/2$, or for the even number k larger than 6.⁴ In order to investigate whether a

³ These quantities are of order $M u_i^2$ and M^2/r_i , where the index $i = 1, 2$ refers to the core and halo domains (here $M_1 \sim M_2 \sim M/2$). Their relative values depend on the mean velocity and on the size of the fluid in each region. We observe numerically that the velocity in the halo is much smaller than in the core (and the inverse for the size r_i).

⁴ The kinetic energy behaves as $E_{\text{kin}} \sim \rho_c u_0^2 r_0^3$. Using $\rho_c \sim (-t)^{-2}$, $r_0 \sim (-t)^{2/\alpha}$ and $u_0 \sim (-t)^{-1+2/\alpha}$, we get $E_{\text{kin}} \sim (-t)^{10/\alpha-4} \sim -W$. Therefore, the divergence of the kinetic energy $E_{\text{kin}} \rightarrow +\infty$ in Eq. (121) could compensate the divergence of the gravitational energy $W \rightarrow -\infty$. However, numerical simulations show that W dominates. Therefore, as a result of the conservation of the energy, the collapse of the core ($W \rightarrow -\infty$) is associated with an increase of the temperature of the system ($T \rightarrow +\infty$).

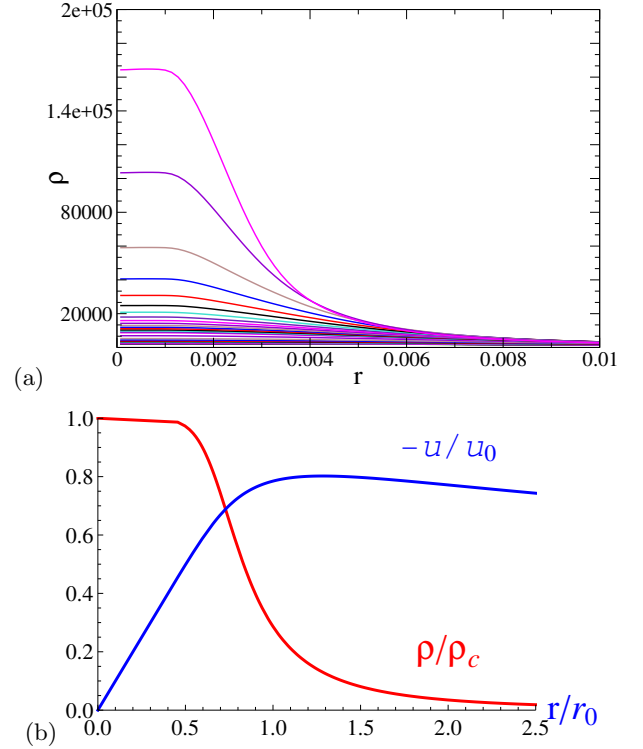


Fig. 7. Density in the core domain before collapse: (a) Numerical solutions of the MEP model ($\rho(r, t)$ increases with time); (b) Invariant profiles (126)-(128) versus r/r_0 of the self-similar pressureless Penston-type solution with $k = 8$.

self-similar solution of the form (118), (119) and (122) agrees with the numerical results, let us first look at the temperature behavior in the post-Painlevé regime before the divergence, for $t_s < t < t_*$, where $t_s \simeq 0.60$ and $t_* \simeq 0.684$. Restoring the initial notations, equation (122) writes

$$T(t) = T(t_s) \left(\frac{t_* - t}{t_* - t_s} \right)^{a(k)} \quad \text{with} \quad a(k) = \frac{15 - 2k}{3k}. \quad (123)$$

The best fit with the numerical results occurs for $a = -0.074$ which is chosen in the insert (green line) of Figure 5-(b). This value corresponds to $k = 8.4$, or $\alpha = 2.5454$, indicating that the integer value $k = 8$ is a possible candidate. The corresponding exponent

$$\alpha(8) = \frac{48}{19} \quad \text{implying} \quad a(8) = -\frac{1}{24} \quad (124)$$

chosen to draw the green line superposed to the full curve $T(t)$ gives a good fit with the numerical curve. For the value $k = 8$, the temperature diverges at the collapse time as

$$T(t) \propto (t_* - t)^{-1/24}. \quad (125)$$

Let us now check and see if the radial solutions $u(r, t)$ and $\rho(r, t)$ also display a self-similar behavior with invariant functions corresponding to the value $k = 8$ suggested by the temperature behavior. The numerical density curves $\rho(r, t)$ for increasing time values are shown in

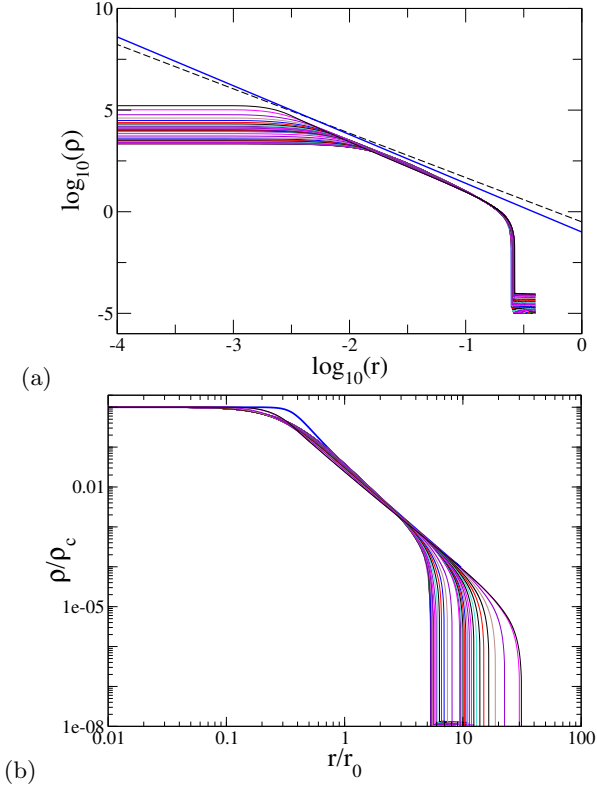


Fig. 8. Density $\rho(r, t)$ before core collapse in \log_{10} scale (numerical solution of the MEP equations). In (a) the thick straight lines display the slopes $\alpha(8) = -48/19$ (solid blue) and $\alpha(4) = -24/11$ (dashed black) respectively; in (b) the numerical solutions $\rho(r, t)/\rho(0, t)$ versus $r/r_0(t)$ for $\alpha(8)$ are superposed to the invariant function (126)-(127) in blue thick line.

linear and logarithmic scales in Figures 7-(a) and 8-(a) respectively. The latter shows an asymptotic behavior $r^{-\alpha}$ which agrees with the the slope $\alpha(8) = 48/19$ reported above the curves (blue straight line) of Figure 8-(a). For comparison, the slope $\alpha(4) = 24/11$ of the CEP model is plotted in dashed (black) line. Note that in both cases (CEP and MEP models) the value of α is larger than 2 contrary to Penston's isothermal solution [24] deduced by assuming that pressure and gravity forces keep the same order of magnitude until the collapse.

The whole self-similar solution $(U(\cdot), R(\cdot))$ can be derived either by solving the two coupled differential equations (102) and (103) of Paper I, or by using the parametric solution given in Appendix B.1 of Paper I which generalizes Penston's pressureless solution [24], namely

$$\frac{\rho(r, t)}{\rho_c(t)} = \frac{3}{3 + 2(3 + k)y + (3 + 2k)y^2}, \quad (126)$$

$$\frac{r}{r_0(t)} = y^{1/k}(1 + y)^{2/3}, \quad (127)$$

$$\frac{u(r, t)}{u_0(t)} = -\frac{y^{1/k}}{(1 + y)^{1/3}}, \quad (128)$$

where $y(t) \propto t_*/(t_* - t)$ goes from 0 to $+\infty$.

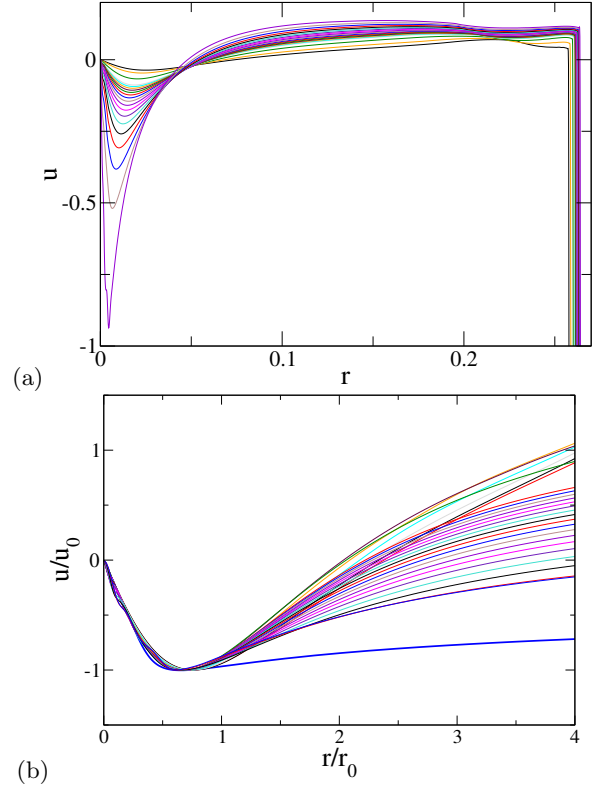


Fig. 9. (a) Velocity $u(r, t)$ for $t_s < t < t_*$ in the whole star (the modulus of the extremum increases with time); (b) Velocity ratio $-u(r, t)/u_0(t)$ versus $r/r_0(t)$ compared to the invariant parametric solution (126)-(128) applying to the core for $k = 8$ (blue thick line).

The exponent of the MEP model, $\alpha(8) = 48/19$, corresponds to the on-axis behavior of the function $R = R_0 + R_8\xi^8 + \dots$, whereas with the CEP model we found $k = 4$, $\alpha(4) = 24/11$ and $R = R_0 + R_4\xi^4 + \dots$. The invariant functions $(U(\cdot), R(\cdot))$ are drawn in Figure 7-(b) in linear scale.

To compare the numerical curves with the functions $(U(\cdot), R(\cdot))$ we define a time dependent core radius $r_0(t)$ by the relation $\rho(0, t)r_0(t)^\alpha = 1$ and plot $\rho(r, t)/\rho(0, t)$ and $u(r, t)/u_0(t)$ versus $r/r_0(t)$. Using this procedure, the density curves merge quite well (in the core domain) into the theoretical solution of equations (126) and (127) plotted in blue line for $k = 8$, as illustrated in Figure 8-(b).

The merging of the velocity curves into a single one U is not as good, except close to the center, for $r \leq r_0(t)$, see Figure 9-(b). At larger radii, the numerical curves separate, approaching asymptotically the solution U (blue line) in the core as time tends to t_* . Compared to the CEP results, where the self-similar behavior was also better for the density than for the velocity, we note that here the non-merging region concerns the right part of the curve only (compare Figure 9-(b) with Figure 14 of Paper I). We attribute this effect (at large radii) to the fact that the velocity has to change its sign at the internal surface of the halo r_h , which enforces the slope of the velocity

at the beginning of the self-similar regime when the ratio r_0/r_h is not small.

4.2 Halo: No self-similar solution

The velocity curves presented in Figure 9-(a) clearly illustrate the simultaneous inward/outward motion of matter in the time interval $t_s < t < t_*$, where the velocity is negative in the core, and *positive* in the halo, with a modulus increasing with time in both parts. During the self-similar growth of density and inward velocity in the core, what happens in the halo? Is the solution self-similar there? We shall see that the answer is NO.

First, we note that the velocity and density diverge only in the core while they remain finite in the halo, as illustrated in Figure 10 which zooms in Figure 9-(a) in the halo region. Moreover, during the time interval $t_s < t < t_*$, the halo gains a radial extension of about 20%, a small evolution compared to the strong shrinking of the core. These two observations seem to indicate that the expansion of the halo is still in a preliminary stage when the core collapses. However, one may ask if the solution is self-similar in the halo before the core collapse (or if it will become self-similar after the collapse, a property investigated in the next section, while not studied numerically). Looking at this possibility, we search for a self-similar solution for a dilute medium by neglecting the self-gravity, so the Euler equations (1) and (2) reduce to

$$\frac{\partial \rho}{\partial t} + \frac{1}{r^2} \frac{\partial}{\partial r}(r^2 \rho u) = 0 \quad (129)$$

and

$$\frac{\partial u}{\partial t} + u \frac{\partial u}{\partial r} = -\frac{1}{\rho} \frac{\partial P}{\partial r}. \quad (130)$$

We assume that the equation of state is purely isothermal⁵ so that

$$P = \rho T(t). \quad (131)$$

The pressure increases because the temperature $T(t)$ increases with time when the core shrinks self-similarly, as described just above if k , an even number, is larger than 6 in equation (123). We take

$$T(t) \propto (-t)^a \quad (a < 0). \quad (132)$$

We neglect the size of the core as compared to the size of the halo (this is marginally valid since $r_h = 0.05$ and $r_c = 0.26$).

We first look for a self-similar solution of the form

$$\rho(r, t) = (-t)^\beta R \left(r(-t)^{\beta/\alpha} \right), \quad (133)$$

⁵ Since the initial density is larger than unity in the main part of the halo, we shall consider that the equation of state (52) may be approximated by equation (131). This was a problem to build equilibrium solutions with a finite mass but this is not a problem if we consider dynamical solutions.

$$u(r, t) = (-t)^\delta U \left(r(-t)^{\beta/\alpha} \right). \quad (134)$$

The exponents are linked by the relations

$$\beta/\alpha + \delta + 1 = 0, \quad (135)$$

$$\delta - 1 = a + \beta/\alpha. \quad (136)$$

Assuming that the mass in the halo $M_h = 4\pi \int \rho(r', t) r'^2 dr'$ is approximately constant during this short time interval (an approximation not really fulfilled here where matter comes from the inside layer, see Figure 10 where the zero-velocity radius $r_h(t)$ decreases from 0.075 to 0.05), we obtain

$$\alpha = 3. \quad (137)$$

Then we find

$$\beta = -3 \left(\frac{a}{2} + 1 \right), \quad \delta = \frac{a}{2}. \quad (138)$$

Using the value $a = -1/24$ from equation (124), we obtain a self-similar solution which diverges at t_* , the density increasing as $(-t)^{-47/16}$, the velocity as $(-t)^{-1/48}$, and the radius shrinking to zero as $(-t)^{47/48}$. This clearly disagrees with the numerical results where the dimension of the halo increases by a factor 1.2, the velocity barely increases and the density decreases. To explain the irrelevance of the above scalings for our model, we have to notice that they are derived within the hypothesis that the pressure dominates over gravity, an hypothesis that could be irrelevant at this stage because the halo is not yet dilute enough. Precisely, the density in the inner part of the halo is approximately equal to 30 (which is the initial density at $r = 0$ in the canonical case where gravity dominates) and the gravitational attraction by the core is not negligible with respect to the self-gravity forces in the halo because the mass of the core is approximately equal to the mass in the halo, see Figure 2-(b), and the halo is still close to the core: its internal radius ($r_h \sim 0.05$) is noticeably smaller than its size ($r_c - r_h = 0.21$).

To go further in the investigation of self-similar solutions in the dilute gas, and motivated by the linear behavior of the velocity profile for $t \simeq t_s$ in Figure 10, we perform a more precise study of the self-similar solutions of equations (129)-(130) of the form (133) and (134) under the assumption that the velocity increases linearly with the distance, namely with the ansatz

$$\rho(\mathbf{r}, t) = \frac{M}{R(t)^3} f \left[\frac{\mathbf{r}}{R(t)} \right], \quad \mathbf{u}(\mathbf{r}, t) = H(t) \mathbf{r}. \quad (139)$$

This study is reported in Appendix C for an equation of state $P = K(t) \rho^\gamma$. There, we show that the radius obeys the differential equation

$$\ddot{R} R^{3\gamma-2} = (t_* - t)^a. \quad (140)$$

In Appendix C.7.1 we consider first solutions of the form

$$R(t) = A(t_* - t)^q. \quad (141)$$

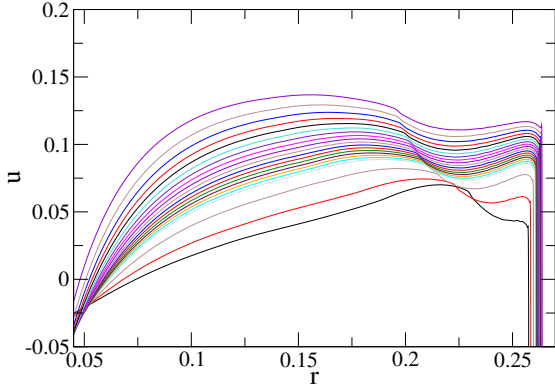


Fig. 10. Velocity versus radius in the halo for $t_s < t < t_*$ (the maximum increases with time).

For $\gamma = 1$, we show that a solution of the form (139) exists only for $a < -2$. Therefore this solution with $u \propto r$ is incompatible with our numerics where we found $a = -1/24$. This result confirms that a gravity-free self-similar solution of the form (133)-(134) is not appropriate to describe the dynamics of the halo during the strongly nonlinear regime before the core collapse.

On the other hand, assuming that gravity dominates pressure does not fit the numerics as well (because this hypothesis gives the same exponents as the ones found for the collapse). Finally, assuming that gravity and pressure forces are of the same order of magnitude leads to the exponents values $\alpha = -\beta = 2$ and $\delta = a/2$ which do not fit our numerical results. We conclude that the halo does not follow a self-similar evolution of the form of equations (133) and (134) in the pre-collapse regime, whatever is the ratio between the gravity and the pressure forces.

Secondly, in Appendix C.7.3, we consider another type of gravity-free self-similar solution which also obeys (140), but we replace equation (141) by the condition that the radius of the star $R(t)$ increases and tends to a constant B at t_* , i.e.,

$$R(t) = B + \epsilon(t) \quad \text{with} \quad \epsilon(t)_{t \rightarrow t_*} \rightarrow 0. \quad (142)$$

In that case, we show that the solution exists and is valid provided that $-2 < a < 0$. The velocity of expansion \dot{R} takes a finite value at time t_* when $a > -1$, and the density decreases as $t \rightarrow t_*$. These two properties agree with our numerical results, Figure 10, although the starting hypothesis $u = H(t)r$ is definitely not fulfilled. In summary a gravity-free self-similar solution associated to diverging temperature and non-diverging radius exists, but it is irrelevant to describe the dynamics of the halo in the pre-collapse regime because it supposes that the velocity increases linearly with the radius for $t_s < t < t_*$, which is not observed in our simulation.

5 Self-similar dynamics just after the singularity (post-collapse regime)

In this Section, we present self-similar solutions for the core and the halo just after the singularity time t_* (as in

the previous Section, we take it as the origin of time). In the core region, we assume that gravity forces overcome pressure forces, as it was stated in the pre-collapse regime. On the other hand, we propose a self-similar solution for the halo which is based on the opposite assumption (pressure overcoming gravity). This solution may be valid soon after the singularity, when the star is very hot and the pressure in the halo is larger than the gravity because the expansion already took place. We did not perform any numerical simulation to check whether these self-similar solutions agree with the MEP model, particularly because of the formation of a singularity at $r = 0$ (Dirac peak) in the core plus the lack of knowledge on the temperature evolution in the halo (assumed here of the form $T(t) \propto t^a$ where the exponent $a > 0$ is unknown).

5.1 Solution in the core domain

We outline here the derivation of the solution in the core which is similar to the solution of the CEP model but with a different value of the exponent α ($\alpha_{\text{MEP}} = 48/19$ instead of $\alpha_{\text{CEP}} = 24/11$). We emphasize that the density does not write as a Dirac distribution at the singularity time t_* , but as a power law $\rho(r, 0) \propto r^{-\alpha}$ which yields a mass equal to zero at the center because the mass integral converges at $r = 0$ for $\alpha < 3$.

At very short times after the collapse, we assume that the inward motion follows a free fall dynamics in the core region. The situation is then qualitatively the same as in the CEP model, and looks (mathematically) like the one of the dynamics of the Bose-Einstein condensation where the mass of the condensate begins to grow from zero *after* the time of the singularity [25, 26]. A self-similar solution exists which is the one derived in [3] but for the value of the exponent α found here, equation (124). We recall that the main change with respect to the pre-collapse study amounts to adding to the equations of density and momentum conservation, an equation for the mass at the center $M_c(t)$ (with $M_c(0) = 0$). The mass flux across a sphere of radius r being $J = 4\pi r^2 \rho(r) u(r)$, the equation for $M_c(t)$ is

$$\frac{dM_c}{dt} = [-4\pi r^2 \rho(r) u(r)]_{r \rightarrow 0}. \quad (143)$$

Therefore, the equations one has to solve now are the same as before,

$$\frac{\partial \rho}{\partial t} + \frac{1}{r^2} \frac{\partial}{\partial r} (r^2 \rho u) = 0, \quad (144)$$

$$\frac{\partial u}{\partial t} + u \frac{\partial u}{\partial r} = -\frac{GM(r, t)}{r^2}, \quad (145)$$

plus the mass inside a sphere of radius r

$$M(r, t) = 4\pi \int_0^r dr' r'^2 \rho(r', t) + M_c(t). \quad (146)$$

These equations after singularity include the whole set of equations leading to the singularity. Moreover, the solution at t_* has the same asymptotic behavior on both sides

of the singularity. It follows that the scaling laws are the same before and after t_* . At very short times after t_* taken as the origin of time, only the solution very close to $r = 0$ is changed by the occurrence of a finite mass at $r = 0$ which is very small. We look for a self-similar solution of equations (144)-(146) with $\rho(r, t)$ and $u(r, t)$ having the same exponents as before collapse:

$$\rho(r, t) = t^{-2} R_+(rt^{-2/\alpha}), \quad (147)$$

$$u(r, t) = t^{-1+\frac{2}{\alpha}} U_+(rt^{-2/\alpha}), \quad (148)$$

plus another scaling for $M_c(t)$:

$$M_c(t) = K_M t^b, \quad (149)$$

where $\alpha = 48/19$ and b is a positive exponent to be found. The two terms on the right-hand side of equation (146) are of the same order of magnitude with respect to t if

$$b = \frac{6}{\alpha} - 2, \quad (150)$$

a positive exponent as it should be (recall the condition that α is less than 3). For $\alpha = 48/19$, we get $b = 3/8$. Therefore, the mass at $r = 0$ and the core radius evolve with time t (positive) as

$$M_c(t) = K_M t^{\frac{3}{8}}, \quad R_c(t) \sim t^{\frac{19}{24}}, \quad (151)$$

in this self-similar post-singularity regime. We refer the reader to [3] for additional information about this self-similar solution (see, in particular, the explicit analytical solution given in Appendix B of [3]).

The evolution of the temperature of the system in the post-collapse regime where the core is a mathematical singularity (Dirac peak) is not clear. Indeed, the divergence of the potential energy of the core would imply an infinite temperature (for global energy conservation). However, if we replace the singular core by a relativistic compact object such as a neutron star, we can get an estimate of the temperature by the relation $k_B T \sim M_c c^2$ leading to the scaling

$$T(t) \propto t^{3/8}. \quad (152)$$

We shall consider this law of evolution of the temperature in the following section and in Appendix C.6.

5.2 A self-similar solution for the halo

We assume that the energy released during the collapse of the core heats the halo and provides its expansion. Indeed, as the gravitational energy W of the core decreases (and becomes very negative), the temperature T of the halo and its macroscopic kinetic energy E_{kin} increase and become very large ($T \sim E_{\text{kin}} \sim -W$) as a result of energy conservation. Therefore, the pressure inside the halo can be high enough to accelerate its expansion. More precisely, we assume that the pressure forces in the halo are stronger than the gravity forces, a condition which will be

checked *in fine*. For the sake of generality, we assume that the halo has a polytropic equation of state of the form

$$P = K(t) \rho^\gamma, \quad (153)$$

where $K(t)$ is an increasing function of time. The isothermal case is recovered for $\gamma = 1$ and $K(t) = T(t)$.

In Appendix C we show that a self-similar solution exists within such a frame, a question which is interesting from a mathematical point of view in addition to its potential applicability to the expansion of the halo in the supernova problem. The self-similar solution has a Tsallis [27] invariant density profile (reducing to a Gaussian for $\gamma = 1$) with a typical radius $R(t)$ and a velocity field which increases linearly with the radius r . The halo expands with time, as expected, its size $R(t)$ evolving according to the second order differential equation

$$\ddot{R} R^{3\gamma-2} = K(t). \quad (154)$$

Equation (154) shows that the expansion rate $\dot{R}(t)$ is time dependent, contrary to what is generally admitted in the first stage of the expansion, an important point which is discussed below. The case where $K(t) = K$ is independent of time corresponds to

$$\ddot{R} = \frac{K}{R^{3\gamma-2}}. \quad (155)$$

This equation is similar to Newton's law for a particle in a potential of the form $V(R) = [K/3(\gamma-1)]R^{-3(\gamma-1)}$. It is studied in Ref. [28] by analogy with cosmological models (the isothermal case $\gamma = 1$ is treated specifically in Appendix C.5 of the present paper and asymptotic results valid for an arbitrary index γ are also given in that Appendix). Here, we assume that $K(t) = t^a$, where a can be of any sign for the sake of generality. In that case, the radius of the halo obeys the differential equation

$$\ddot{R} R^{3\gamma-2} = t^a. \quad (156)$$

The asymptotic behavior of the solution of this equation is studied in Appendix C.6. Below we illustrate some particular behaviors numerically.

Numerical solutions of equation (156) are presented in Figures 11-(a) and 12-(a) respectively for several values of the exponents a and γ chosen for their role in the late time dynamics. In all cases the expansion rate \dot{R} is clearly time dependent, see the curves of Figures 11-(b) and 12-(b) which display the kinetic energy $E_{\text{kin}} \propto \dot{R}^2$. This result differs from the common description of the remnant motion just after the explosion (supposed to expand with a constant velocity due to the conservation of kinetic energy). We shall return to this so-called “free expansion regime” in the next Section. Here, we look if there is a range of parameter values (a and γ) such that the self-similar solution has an expansion rate which tends *asymptotically* to a constant value. In Appendix C.6.3 we show that such an asymptotic solution exists, and fulfills our assumptions that pressure is stronger than gravity, provided that

$$\frac{3+a}{3} < \gamma < \frac{4+a}{3}. \quad (157)$$

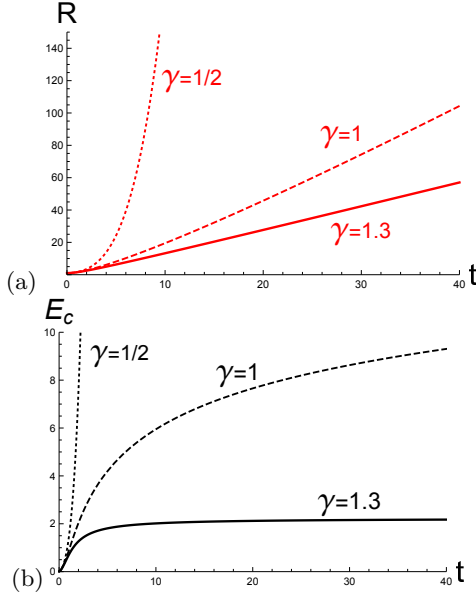


Fig. 11. Solution of equation (156) for the case of an adiabatic expansion ($a = 0$) with initial conditions $R(0) = 1$ and $\dot{R}(0) = 0.1$. (a) Radius of the halo $R(t)$; (b) Kinetic energy $E_{\text{kin}}(t) \sim \dot{R}(t)^2$. In (a) the solid line for $\gamma = 1.3$ shows an asymptotic constant rate, the dashed line for $\gamma = 1$ displays an expansion rate increasing with time as $t \log(t)^{1/2}$, and the dotted line for $\gamma = 1/2$ evolves as $R(t) \sim t^4$ asymptotically. Same legend for curves (b).

In that case, the asymptotic behavior of the velocity is given by

$$\dot{R}(t) \simeq v + \frac{1}{v^{3\gamma-2}} \frac{t^{-3(\gamma-1)+a}}{a-3\gamma+3} + \dots \quad (t \rightarrow +\infty). \quad (158)$$

Other solutions with a different asymptotic behavior, that are valid for values of γ in a range different from equation (157), are given in Appendix C.6. Assuming an adiabatic expansion and an homogeneous entropy inside the halo, amounts to considering the case $a = 0$ (see the next Section). In that case, the condition of validity of the solution (158) corresponding to $R \sim vt$ is $1 < \gamma < 4/3$. For example, for $\gamma = 1.3$, we can check on Figure 11 that the asymptotic expansion rate is constant. By contrast, for $1/3 < \gamma < 1$ the radius increases as $R(t) \propto t^{2/(3\gamma-1)}$ (see Appendices C.5.2 and C.6.1) and for $\gamma = 1$ it increases as $R(t) \propto t\sqrt{\ln t}$ (see Appendix C.5.1). More generally, for $\gamma = 1$, the asymptotic expansion rate is constant when $-1 < a < 0$ while the radius increases as $R(t) \propto t^{(a+2)/2}$ when $a > 0$. In particular, for $\gamma = 1$ and $a = 3/8$ (see the end of Sec. 5.1), the radius increases as $R(t) \propto t^{19/16}$ (see Appendix C.6.1) which is not very far from a linear behavior.⁶ Note that for an ideal gas the exponent γ is equal to unity for an isothermal transformation only, otherwise

⁶ The linear behavior characterizes what is generally called free expansion, understood as the propagation of the remnant with constant kinetic energy, at the very beginning of the expansion when the pressure of the interstellar gas is negligible, before accumulated mass of this gas affect the expansion.

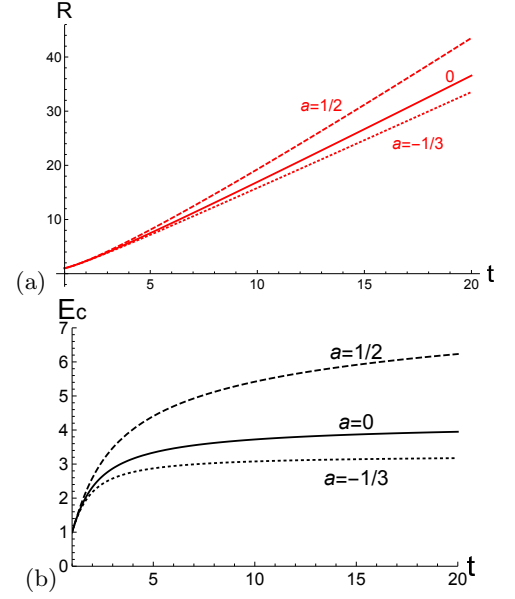


Fig. 12. Solution of equation (156) versus time with initial conditions $R(1) = \dot{R}(1) = 1$ for $\gamma = 1.2$. (a) Radius of the halo $R(t)$; (b) Kinetic energy $E_{\text{kin}} \propto \dot{R}(t)^2$. We have taken a equal to $-1/3$ (dotted), 0 (solid), and $+1/2$ (dashed), respectively. In each case the kinetic energy tends to a constant for $t \rightarrow +\infty$.

one has $\gamma > 1$. This is because an adiabatic transformation implies $\gamma = c_p/c_v$ with c_p larger than c_v , and other transformations (called “polytropic”) are intermediate between adiabatic and isothermal. Therefore we chose a value of γ larger than unity to illustrate the role of the exponent a on the dynamics of the solution. The solution of equation (156) is shown in Figure 12 for $\gamma = 1.2$ and various values of the exponent a which satisfy the condition (157). In addition to the adiabatic case ($a = 0$), we have chosen a positive ($a = 1/2$) and a negative ($a = -1/3$) value of the exponent a . In all cases, the late time dynamics displays the condition of asymptotic constant kinetic energy, but with different time scales. In Figure 12-(b), the velocity tends to a constant plus a term decreasing as $t^{-0.93}$, $t^{-0.6}$, and $t^{-0.1}$ for the dotted, solid and dashed line respectively. Note that if the self-similar solution proposed here could describe the first stage of the expansion of the halo, we expect that it merges ultimately with the non self-similar Burgers solution suggested in Section 6 which displays shocks.

6 Isentropic expansion of the halo and shock formation

6.1 Physics of the free expansion stage

Here, we consider the expansion of the remnants, namely the gas ejected by the explosion of a supernova. We shall assume that the remnant is a dilute gas, although much denser than the interstellar medium. We consider a general equation of state but, as we show below, the pressure is irrelevant for the expansion of a dilute gas. The study

of the remnants is of interest because it represents the last stage of the evolution following a supernova explosion which should be matched with the previous stage of the supernova. In addition, those remnants have been observed both on SN1987A and for a number of supernovae having exploded in our Galaxy not too long ago. Lastly, this study is of interest also because it is one of the few instances where a lab-model could be looked at on Earth with some relevance for an astrophysical problem.

We shall neglect a set of perhaps crucial phenomena, namely plasma effects due to the finite electric conductivity of the expanding gas (this yields Laplace forces which could supersede inertia and gravity in the expanding gas). We shall also assume spherical symmetry, not displayed by the observed remnants, except for their large scale structure. As shown later, asphericity is not so crucial from the point of view of the present analysis.

We consider what is called sometimes in the literature the “free expansion stage” following the supernova explosion, when the ejecta are believed to expand freely in space and cool adiabatically because of their expansion. This stage begins after the formation of the neutron star (if any is formed) and when the temperature, pressure and density of the remnants are small enough, see below. It should last until the density of the remnants becomes of the order of magnitude of the density of the interstellar gas. It seems that this is considered as a rather uneventful stage of the expansion, although we believe that this stage of adiabatic cooling is of primary interest. Here, we point out that in order to create structures in an expanding gas volume, as observed in the remnants, there is no need to have interaction with an outside interstellar gas because shocks can occur even within the dynamics of the expanding gas. As we shall show, this occurrence of shocks depends on the initial distribution of the fluid velocity *inside* the remnants: if the radial velocity is larger for a given radius than for a larger one, a shock forms because the larger velocities overcome the slower ones. This shock has its own dynamics related to the conservation relations. Lastly, this early stage of the expansion is, by far, the one that is the best known experimentally because it is a stage where the remnants are still far more luminous than the rest of the Galaxy. Based on the existence of such internal shock waves, we suggest an explanation for the very sharp luminous rings observed in the remnants of SN1987A. Therefore, we believe it is of interest to try to understand this “free expansion stage”.

A basic question concerning the free expansion is the validity of its fluid mechanical description. This question concerns the expanding matter, but could also concern the interstellar medium. The validity of such a picture requires that the mean free path of molecules, ions, electrons and atoms in the expanding gas (or in the interstellar medium) is much smaller than the length scale of the structure under consideration. If this is not the case, one has what is called a dust gas, without interaction between the particles other than possibly gravitation. In such a dust gas, the conservation of entropy does not occur, velocity fields with more than one value at a given point are perfectly possi-

ble, and shock waves are absent. Here, we assume that the expanding matter is dilute, but not infinitely dilute, with a mean free path far smaller than its size. Therefore, it can be described as a fluid at very large Mach number, in the sense of regular fluid mechanics, namely with a single valued velocity field. The constraint of single valued velocity field explains the formation of shock waves inside this expanding gas, before any interaction with the interstellar medium, as discussed below.

For the interstellar medium, a fluid mechanical description is questionable. According to Spitzer [29,30], its mean free path in the usual sense is of the order of the size of the Galaxy. It is about 500 pc for a 2 MeV proton moving in a gas of neutral hydrogen atoms of density of order one atom per cubic centimeter, that should forbid to consider it as a fluid. However, Spitzer notices that, because of the existing magnetic field in the Galaxy, the gyration radius of protons is far smaller than their mean free path, which could reduce by orders of magnitude the mean free path of protons. This could well be, but we must notice that charged particles move freely along the lines of the magnetic field making this reduction of the mean free path not so efficient. Moreover, as noticed by Spitzer, the energy density of the galactic magnetic field is well below the one of the expanding gas so that it is not clear that the electric currents due to the galactic magnetic field are able to slow down this expanding gas.

Another question is the interaction between the molecules of the expanding bubble. As it expands, its density decreases and it should enter in the so-called Knudsen regime where the mean free path of atoms and molecules becomes of the same order or bigger than its radius R . This stage comes quite late in the expansion, as shown by the following simple estimate: the radius of the blob is of order $(M_h/\rho)^{1/3}$ although the mean-free path l is of order $l = m/(\rho\sigma)$ where m is the mass of the atoms making the gas and σ is the cross section for the collisions. Therefore, as the density decreases, the mean free path should become larger than the radius of the gas blob, forbidding to describe this gas by the equations of fluid mechanics supplemented by the thermodynamic relations. To put this condition in a dimensionless form, let us introduce the quantity

$$\rho_{\text{Kn}} = m\sigma^{-\frac{3}{2}}, \quad (159)$$

which is the mass density of dense matter, the inter-particle distance of which is of order of $\sigma^{1/2}$. The mean free path becomes of the order of the radius of the cloud when its density is such that

$$\rho = \rho_{\text{Kn}} \left(\frac{m}{M_h} \right)^{\frac{1}{2}}, \quad (160)$$

a very low density compared to usual densities of condensed matter, m/M_h being like the inverse number of atoms in the expanding cloud, surely a very small number.

In summary, we consider below the post-explosion regime where the expanding gas is dense enough to be interacting with itself (the attraction by the core of the exploded

star will also be considered), but not with the interstellar medium, and such that it makes a continuous fluid, not a Knudsen gas.

6.2 Difference with the Sedov-Taylor problem

In this regime, we first point out that a self-similar expansion with gravity and pressure forces included in the equation has to be rejected. Many authors invoke the Sedov-Taylor solution (see Section 106, p. 403-406, of [31] and [32,33,34]) to describe the second phase of the expansion of the remnant. But the Sedov-Taylor solution was derived for the expansion of an explosion releasing energy in another gas. This solution conserves energy only, while mass conservation does not enter into the solution because the initial mass is mixed with the infinite mass around. Therefore Sedov-Taylor is not suitable here because, in our description of the free expansion stage, the remnant is an entity which exchanges neither energy nor mass with the interstellar medium. Then we have to impose the constraints of conservation of mass and energy for the remnant. In our case, self-similarity of the *free expanding bubble*, if it exists, requires to neglect some physical effects, as it was done for the description of free fall of dense molecular clouds where the pressure forces were assumed to be negligible with respect to the gravity forces.

Below, we consider two cases, first when gravity is negligible compared to pressure, secondly when both gravity and pressure are negligible. In the former case, we show that the conservation of mass and energy is compatible with a self-similar solution only for the case $\gamma = 1$ which corresponds to an isothermal process, not to an adiabatic one. This solution must be rejected since $c_p = c_v$ is unphysical for a dilute gas. In the latter case, we derive rather straightforwardly an approximation of the fluid equations of Burgers-type, which is well-known to yield shocks. This equation has a simple solution which can be extended beyond situations of perfect spherical symmetry. This solution differs from the one of free fall of a dust gas in a few points. First, the Burgers solution is not self-similar and depends on the initial conditions contrary to the free fall solution. Secondly, if those conditions are such that a shock wave is created, the subsequent evolution couples mass, energy and momentum conservation by the Rankine-Hugoniot relations which link the flux across the shock waves and yield ultimately their trajectory. Somehow, dynamics of mass and energy (the two being linked by the adiabatic condition) are enslaved to the velocity field when this one is smooth (before the shock), but actively enters into the dynamics when shock waves are formed.

The equations for an inviscid compressible ideal fluid in spherically symmetric situations, including self-gravitation, read (see Section 6 of [31]):

$$r^2 \frac{\partial \rho}{\partial t} + \frac{\partial(\rho u r^2)}{\partial r} = 0, \quad (161)$$

$$\frac{\partial u}{\partial t} + u \frac{\partial u}{\partial r} = -\frac{1}{\rho} \frac{\partial P}{\partial r} - \frac{4\pi G}{r^2} \int_0^r dr' r'^2 \rho(r'), \quad (162)$$

$$r^2 \frac{\partial}{\partial t} \left(\frac{1}{2} \rho u^2 + \rho \varepsilon \right) + \frac{\partial}{\partial r} \left[\rho u r^2 \left(\frac{1}{2} u^2 + w \right) \right] = 0, \quad (163)$$

where ρ is the mass density, u the radial velocity, ε the internal energy per unit mass, $w = \varepsilon + p/\rho$ the enthalpy per unit mass and G is Newton's constant. Equation (163) can be transformed into the condition that the flow is isentropic

$$\frac{\partial(r^2 s \rho)}{\partial t} + \frac{\partial}{\partial r} (u r^2 s \rho) = 0, \quad (164)$$

where s is the entropy per unit mass such that $d\varepsilon = T ds + (p/\rho^2) d\rho$. To take advantage that the flow is isentropic, one uses as thermodynamic variables the density ρ and the entropy s . Therefore, the pressure P is a function of those two quantities, $P(\rho, s)$. If the heat capacities of the gas are independent of temperature, Laplace's relation between pressure and density reads

$$P = K(s) \rho^\gamma, \quad (165)$$

where $\gamma = c_p/c_v$ is the ratio of heat capacities at constant pressure and constant volume (for an ideal gas undergoing an adiabatic process). For the sake of generality, we did introduce a constant $K(s)$ depending explicitly on the entropy s because it is possible to have an initial state of non-uniform entropy. However, we shall assume later that the entropy is initially uniform, and try to find a possible self-similar solution of the above set of equations for a gas bubble expanding *in vacuo*. To that purpose, we look for solutions depending on time and radius as $F(r, t) = r^a f(rt^b)$, where a and b are exponents to be derived from the equations, with a depending on the field F under consideration (that is either ρ , u or s) although b is the same for all fields. Moreover $f(\cdot)$ is a numerical function with values of order one when its argument is of order one.

In the frame of a perfect gas expanding adiabatically, equation (165) requires that the pressure tends to zero as the density does. Moreover the pressure depends on the temperature as $P \sim T^{c_p/(c_p - c_v)}$ and $c_p > c_v$, which implies that the absolute temperature of the gas tends to zero as well. Therefore, the internal energy of the gas, being proportional to T , must also tend to zero. Moreover, the gravitational energy in equation (5) tends also to zero because the typical dimension of the halo becomes very large (see below the condition for neglecting the gravitation with respect to pressure forces). We shall assume that the isentropic expansion starts after this (short) transient, when the internal and gravitational energies are almost wholly converted into kinetic energy, so that the density of energy per unit mass is of order ρu^2 after this conversion has been achieved. In summary, we assume that the condition of conservation of total energy amounts to imposing that the order of magnitude of the velocity u is constant during the isentropic expansion.

6.3 No self-similar expansion without gravity

Let us insert the self-similar solution

$$\rho(r, t) = r^a R(rt^b), \quad u(r, t) = r^c U(rt^b), \quad (166)$$

in the equations of perfect fluids with the pressure-density relation (165) and neglect the gravitational term. For an expanding solution, one must have $b \leq 0$. From mass conservation, the integral of $\rho(r, t)$ over the whole space must be constant, which implies

$$a = -3. \quad (167)$$

The two terms on the left-hand side of equation (162) are of the same order of magnitude if the condition

$$b(1 - c) = -1 \quad (168)$$

is fulfilled. As noted above, the (reasonable) condition of conservation of kinetic energy requires $c = 0$ which ensures a constant order of magnitude of the velocity field. In this case, the relation (168) reduces to

$$b = -1 \quad (169)$$

which means that the size of the shell expands linearly with time, as $R(t) = vt$. This solution corresponds to what is generally called the “free (or Joule) expansion stage” in the literature [35]. Lastly, imposing that the pressure gradient divided by ρ , with $P = K(s)\rho^\gamma$ and a constant entropy, is minus the acceleration yields

$$b = -\frac{1}{3\gamma - 2}, \quad (170)$$

which agrees with the condition that b is negative if γ is larger than $2/3$. Equations (169) and (170) are compatible for the particular value

$$\gamma = 1 \quad (171)$$

only. However, as mentioned in the previous Section, γ is always larger than 1 in the case of adiabatic or polytropic processes. Therefore, *no physically meaningful self-similar solution of the expanding halo exists for an adiabatic process*. By physically meaningful, we refer to a solution which conserves the kinetic energy and the entropy as assumed above (then γ is larger than unity).

Let us now discuss the range of validity of our hypothesis of negligible gravity forces for self-similar solutions of the form (166). Keeping the relation (168) with equation (170), one finds that the gravitation term scales like

$$\frac{4\pi G}{r^2} \int_0^r dr' r'^2 \rho(r') \sim r^{-2} \sim t^{2b}. \quad (172)$$

This is to be compared with the other terms, for example with the scaling of the acceleration $u_{,t} \sim t^{-1}$ just derived. For any negative value of b the exponent -1 of the acceleration as a function of time is larger than the exponent $2b$ of the gravitational force if $\gamma < 4/3$. Therefore, when looking at the limit of large t , the gravitational force is negligible when γ fulfills the relation

$$\frac{2}{3} < \gamma < \frac{4}{3}. \quad (173)$$

If γ is bigger than $4/3$, the gravitational attraction dominates at large time, then any self-similar solution is expected to evolve toward a collapse.

6.4 Expansion without pressure and without gravity

The alternative to the self-similar solution considered above is to assume that one of the terms in the dynamical equations is negligible with respect to the others, an assumption which changes the scaling laws. Because the pressure tends to zero by adiabatic expansion, it is natural to assume that the pressure term in equation (162) becomes small with respect to the other terms as well as the gravitational interaction in this late stage of the expansion *in vacuo*. This reduces the momentum equation to the simple form

$$\frac{\partial u}{\partial t} + u \frac{\partial u}{\partial r} = 0, \quad (174)$$

an equation well-known since Poisson to have the implicit solution

$$u(r, t) = u_0(r - ut), \quad (175)$$

where $u_0(r)$ is the initial radial velocity. This solution conserves the order of magnitude of u in the course of time, which is consistent with the conservation of energy. The solution in equation (175) is also well-known to become multi-valued after a finite time for a wide range of initial conditions. However, it is easy to find initial conditions remaining single-valued forever by choosing an initial velocity field growing uniformly as r goes from 0 to ∞ , as assumed in the peculiar form (139). An initial condition leading to a multi-valued solution after a finite time yields actually shock waves regularized by viscosity and heat conduction, which could well be what is observed in the remnants of supernovae. Once the velocity field is known as well as the initial distribution of mass density, one can find, at least by implicit relations, the distribution of mass at any later time.

The solution for the density takes the form

$$r^2 \rho(r, t) = \frac{\partial r_0}{\partial r} r_0^2 \rho_0(r_0(r, t)), \quad (176)$$

where $\rho_0(r_0)$ is the initial condition for the density, and where r_0 is the function of (r, t) such that $r_{,t} = u(r, t)$ with the initial condition $r(t = 0) = r_0$, and where $u(r, t)$ is given by equation (175).

At this stage, one should check that the neglected terms are actually negligible in this limit of long times compared to what has been kept. Let us look at equation (162) and compare the terms on the left- and right-hand side in the late stage of the expansion of the gas, that is when r becomes large. The term uu_r , called dynamical pressure term, of order u^2/r , is proportional to $1/r$ because u keeps constant order of magnitude to ensure the conservation of energy. The term P_r/ρ involving the thermodynamical pressure $P \propto \rho^\gamma$ is of order $\rho^{\gamma-1}/r$ with $\rho \sim M_h/r^3$, where M_h is the mass of the expanding cloud. That gives a term of order $1/r^{3\gamma-2}$ decreasing more rapidly with time (as the radius size r increases) than the left hand side term in equation (162) because γ is larger than unity. The gravitational term, namely $-(4\pi G/r^2) \int_0^r dr' r'^2 \rho(r')$, scales like GM/r^2 , where M is the total mass, a constant. Therefore, it decays faster than the term of dynamical pressure, by a factor $1/r$ as r tends

to infinity. This shows that, as assumed, the dynamical pressure is dominant in the regime of a dilute gas. This analysis was based on the fluid equations for a compressible inviscid gas. If this gas becomes highly diluted, it enters the so-called Knudsen regime discussed in Subsection 6.1.

Let us notice again that even though the equations of motion do not include explicitly the temperature (or the entropy) this one is known from the constraint of conservation of entropy (164) where the velocity field is given by the implicit equation (175) and the density derived from the equation of transport of mass (161) or (176). Somehow, one could say that the velocity field of the expanding gas acts a little bit like a piston with an imposed motion such that the gas expands. A related physical phenomenon is the Ranque effect [36] where a gas injected at high pressure tangentially in a cylinder makes a very strong vortex and cools down spontaneously when extracted near the axis of the cylinder where the pressure is low. In the Ranque effect, the cooling occurs not just by expansion as in the theory presented above, but because of the centrifugal force due to the rotation of the gas inside the cylinder.

Because we have in mind the expansion of the mass of a star after it exploded as a supernova, we must consider also the possible effect of a mass remaining at the center of the star, being the rest of the core after the explosion, even though no such dense core has been observed (yet?) in SN 1987A, the best known supernova. This adds another gravity term in equation (162) which becomes

$$\frac{\partial u}{\partial t} + u \frac{\partial u}{\partial r} = -\frac{1}{\rho} \frac{\partial p}{\partial r} - \frac{4\pi G}{r^2} \int_0^r dr' r'^2 \rho(r') - \frac{GM_c}{r^2}, \quad (177)$$

where M_c is the mass of the core, a point mass located at $r = 0$. Contrary to the term of self gravitation, the last term, representing the attraction by the core, diverges near $r = 0$ and so cannot be neglected anymore, at least for r small. Let us suppose that the solution remains like the one derived before, that is with a density decreasing to zero with time, and a radial velocity keeping a constant order of magnitude. Comparing the kinetic energy of a unit mass and the gravitational energy due to the attraction by the core, one finds a critical radius r^* such that if $r > r^*$ the velocity is positive while it is negative otherwise. This radius is $r^* = GM_c/u^2$ where u is the order of magnitude of the velocity. At $r = r^*$ the velocity $u(r)$ changes sign. Because of the scalings, r^* remains of the same order of magnitude, in particular because for r larger than r^* the velocity is directed outward and so no mass is added to the core. Therefore because there is no feeding of mass coming from outside, the radius r^* should stay constant, and the local density tends to zero as it does for r much larger than r^* . For $r \gg r^*$, the blob keeps expanding as explained above because the attraction by the core becomes negligible compared to the dynamic pressure, and the density inside the core tends to collapse on the center, but with a negligible attraction on the expanding gas at radii much larger than r^* , where most the mass is located.

Depending on the initial conditions $u_0(r)$ for the velocity field, the solution of equation (174) may or may

not lead to a finite time singularity. If it does not, the assumptions leading to this equation remain correct for all positive times. If this solution becomes singular at finite time, there is the question of the evolution after the singularity time. As well-known since Riemann, the finite time singularity of the solutions of equation (174) is physically transformed into a solution with a propagating discontinuity, a shock wave, once molecular transport (heat conductivity and viscosity) is taken into account. Notice that such a shock wave is neither the one derived from the Sedov-Taylor model of an expanding gas (the remnant) inside an exterior medium (the interstellar medium) which is supposed to occur at the boundary between the two media, nor the one often referred to in theories of supernovae, which is supposed to occur inside the star just after the core collapse and is believed to play a role in the emission of matter outside. In the present case, the discontinuity propagates also inside the medium where it was born (as in the latter case), but the propagation occurs through an expanding rarefied gas. In our case, we have neglected the pressure term $-P_{,r}/\rho$ in the momentum equation (162), that adds complexity to the standard theory of shock waves. This approximation was based on the fact that the order of magnitude of the thermodynamic pressure P becomes negligible compared to the one of the dynamic pressure (giving rise to the term $uu_{,r}$ in equation (162)).

To neglect the thermodynamic pressure with respect to the dynamical pressure amounts to taking the limit where the velocity of sound, $c_s = \sqrt{p'(\rho)}$, is much less than the actual fluid velocity u , equivalent to the limit of a very large Mach number

$$\mathcal{M} = \frac{u}{c_s} \gg 1. \quad (178)$$

In this limit, one can use the known relations giving the ratio between the thermodynamic parameters on both sides of a shock wave. In the present case, we shall be concerned with the ratio of number densities. As shown in Section 89 of [31], this ratio is, for shock waves of arbitrary Mach number in polytropic gases, given by

$$\frac{\rho_2}{\rho_1} = \frac{(\gamma + 1)\mathcal{M}_1^2}{(\gamma - 1)\mathcal{M}_1^2 + 2}, \quad (179)$$

where the index 1 refers to the upstream part of the shock, and 2 to the downstream part, both being located inside the expanding remnant. In the case of a shock propagating outward, the index 1 refers to the outside and 2 to the inside, while u_1 is the fluid velocity near the shock front on the upstream side in the frame of reference of the shock. Its order of magnitude is the one of the fluid velocity in the expanding gas, much bigger in the low density limit than the speed of sound c_1 on the upstream side. Therefore, as already mentioned, neglecting the thermodynamic pressure is valid in the limit of large Mach number. In this limit, the ratio of densities across the shock takes the finite value $(\gamma + 1)/(\gamma - 1)$, which shows that the accumulation of matter on the shock is limited to a finite ratio. Notice that this ratio is obviously larger than 1 because it is the

ratio of the density on the downstream side (index 2) to the upstream side (index 1). It is equal to 7 for a gas such that $\gamma = 4/3$. It would be interesting to know if a larger effect of mass concentration happens on manifolds where the velocity is more singular than on shock waves, like for instance near the line of merging of two shock surfaces or at points where three shock surfaces meet. An interesting possibility is that such an accumulation of mass and energy increase could explain the observation of rings in SN1987A, with a fair axial symmetry, likely due to the initial rotation of the star. At sufficiently long time after the initial explosion, the shock waves due to the initial conditions for the velocity field likely get an axisymmetrical shape which could result in lines of intersection having this symmetry and so be circles in planes perpendicular to the same axis, the symmetry between the two thin circles being due to a symmetry with respect to the lid plane perpendicular to the axis of rotation of the star.

It is of interest to remark that a shock wave occurring in the expanding gas at decreasing density and temperature is a manner for the system to increase its temperature. In strong shocks (see equation (89.10) of [31]) propagating through polytropic gases, there is a very large increase of temperature on the downstream side. The ratio of the downstream temperature T_2 to the upstream temperature T_1 is given by

$$\frac{T_2}{T_1} = \frac{2\gamma(\gamma-1)}{(\gamma+1)^2} \mathcal{M}_1^2, \quad (180)$$

where \mathcal{M}_1 is the large upstream Mach number. Such a large temperature increase could well explain the observation of a light emitting part of the remnants, particularly near their edge where the effect of an initial velocity difference is more likely to yield a shock wave because of the structure of the solution of the equation (174).

7 Comparison with the canonical description

In this Section, we summarize the main results obtained in this paper, which are valid in the microcanonical ensemble (fixed energy E), and we compare them with those obtained in Paper I, which are valid in the canonical ensemble (fixed temperature T). As discussed in the Introduction, the CEP model gives some results that are identical to those found here for the MEP model, but there are also important differences.

7.1 Series of equilibria

First of all, we recall that the series of equilibria are the same in the canonical and microcanonical ensembles. They are made of all the solutions of equations (16) and (17), stable or unstable, corresponding to the condition of hydrostatic equilibrium. This leads to the spiralling curve of Figure 5 in Paper I and to the spiralling curves of Figure 1 in this paper. However, the stability of the solutions

is different in the microcanonical and canonical ensembles. Using the Poincaré theory [19,20,9], one can show that the series of equilibria is stable in the canonical ensemble before the first turning point of temperature and that it becomes unstable afterward. The instability occurs when the specific heat $C = dE/dT$ becomes infinite, passing from positive to negative values. Furthermore, a new mode of stability is lost at each turning point of temperature as the series of equilibria $\beta(E)$ rotates anticlockwise. The critical point A where the first instability occurs as T decreases (\hat{h}_0 increases) corresponds to a minimum of the temperature. This canonical critical point (saddle-center) has been fully characterized in Paper I. It corresponds to $T_c^{\text{cano}} = 1.546$ and $E_c^{\text{cano}} = 0.378$. Similarly, one can show that the series of equilibria is stable in the microcanonical ensemble before the first turning point of energy and that it becomes unstable afterward. The instability occurs when the specific heat vanishes, passing from negative to positive values. Furthermore, a new mode of stability is lost at each turning point of energy as the series of equilibria $\beta(E)$ rotates anticlockwise. The critical point A' where the first instability occurs as E decreases (\hat{h}_0 increases) corresponds to a minimum of the energy. This microcanonical critical point (saddle-center) has been fully characterized in Section 2.2 of the present paper. It corresponds to $E_c^{\text{micro}} = -0.984142$ and $T_c^{\text{micro}} = 2.22538$. The fact that the onset of instability differs in microcanonical and canonical ensembles ($A \neq A'$) is a manifestation of ensembles inequivalence for systems with long-range interactions [9]. Considering the caloric curve of Figure 1-(b), we note that the region of ensembles inequivalence (between points A and A') occurs in the region of negative specific heats $C = dE/dT < 0$. This is natural because we know from general arguments of thermodynamics that the specific heat must be positive in the canonical ensemble while there is no *a priori* constraint on its sign in the microcanonical ensemble. These results regarding the caloric curve $\beta(E)$ and the notion of ensembles inequivalence are similar to those obtained in the context of box-confined isothermal spheres (see [10,37,18]). We also note that the curves which depict the succession of equilibrium states lead to spirals spinning inversely when the equilibrium radius of the star is plotted versus T or versus E : compare $r_0(T)$ shown in Figure 5 of Paper I with the curve $r_0(E)$ shown in Figure 1-(a) of the present paper. In the canonical ensemble, the series of equilibria is stable until point A, so that the radius always decreases as the temperature decreases (see Figure 5 of Paper I). As a result, we anticipate that the canonical description should give a contraction of the radius of the star (collapse/implosion) after the instability point A. In the microcanonical ensemble, the series of equilibria is stable until point A'. The radius first decreases as the energy decreases, then, after the turning point of radius $r_0 = 0.371$, energy $E = -0.80$, and temperature $T = 1.97$, the radius increases as the energy keeps decreasing (conjointly, in the region of negative specific heat, the temperature increases as the energy decreases). As a result, we anticipate that the microcanonical description should give an expansion of the radius of the star and

an increase of temperature (explosion) after the instability point A' (see Figure 1-(a)).

7.2 Neutral mode

The structure of the neutral mode is different in the canonical and microcanonical ensembles. This has important consequences for the evolution of the star in the collapse regime. The important result is depicted by the spatial profile of the velocity which is negative everywhere for the CEP model illustrated in Figure 13-(a), whereas the velocity clearly changes sign in the star for the microcanonical case (see the curve $S(r)$ drawn in Figure 4-(b)). This shows that the collapse corresponds to a pure inward motion in the canonical ensemble while, in the microcanonical ensemble, the core collapses (inward motion) and the halo expands (outward motion). This result has to be completed by the spatial profile of the density deviation, which displays only one node for the CEP model at the critical point A (see the curve $\delta\rho/\rho$ in the insert of Figure 13-(b)), so the density increases in the core and decreases in the outer layers, whereas in the microcanonical ensemble, the density deviation $\delta\rho/\rho$ at the critical point A' displays two nodes (see Figure 4-(a)), so the density increases in the core and in the halo, while it decreases in the intermediate region.

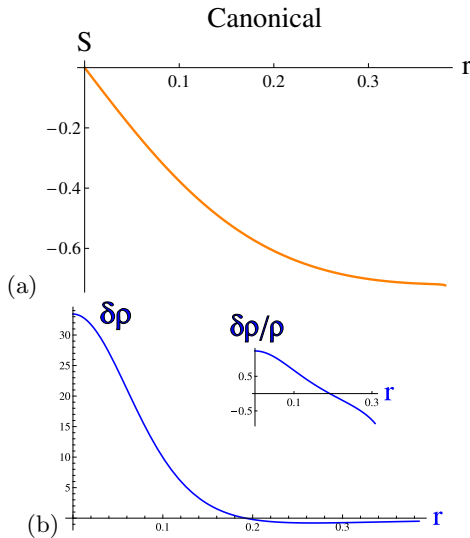


Fig. 13. Radial profile of the first order deviation in the canonical case (CEP model) for (a) the displacement (or velocity), and (b) the density. The insert in (b) shows the presence of a single node.

We note that the above results regarding the structure of the neutral modes in the canonical and microcanonical ensembles are similar to those obtained in the context of box-confined isothermal spheres (see [38] and references therein). However, the box prevents the expulsion of the halo, so the box model is limited in this sense, and the present model, which is unbounded, should be preferred

for astrophysical applications. The above results are also in agreement with general results of thermodynamics applied to self-gravitating systems (see [9] and Appendices A and B of [38]). Indeed, in the canonical ensemble, the system evolves so as to minimize its free energy at fixed mass. Therefore, one expects that the system collapses as a whole and ultimately forms a *Dirac peak* containing all the mass.⁷ Indeed, a Dirac peak has an infinite negative free energy. The collapse of the system is accompanied by a huge decrease of potential energy (W) which overcomes the slower decrease of entropy (or increase of $-TS$). Such an evolution is energetically favorable. On the other hand, in the microcanonical ensemble, the system evolves so as to maximize its entropy at fixed mass and energy. Therefore, one expects that the system takes a *core-halo* structure. Indeed, by collapsing the core and expanding the halo we can make the entropy very large, possibly infinite, while conserving the energy. As the core collapses, its potential energy decreases. Since the total energy is conserved, the kinetic energy of the halo must increase simultaneously. As a result, the halo overheats and is ejected at large distances. Such an evolution is entropically favorable.

7.3 Weakly nonlinear regime

Our weakly nonlinear analysis, whose relevance is confirmed by the numerical solution of the full hydrodynamic equations, is valid during the early stage of the collapse dynamics. It leads to the same Painlevé I equation [see equation (112) here and equation (75) in Paper I] in both canonical and microcanonical models, but the coefficients are different. In Paper I, we obtained $\gamma \simeq 120.2$ and $K \simeq 12.3$, whereas in the present paper we obtained $\gamma \simeq 46.62$ and $K \simeq 1055.98$. Therefore, the amplitude $A(t)$ increases more slowly in the canonical model than in the microcanonical one, compare Figure 8 of Paper I with Figure 5 here. This is related to the fact that the critical density $\rho_0^{(c)}$ is much lower (by a factor 100) in the CEP model with respect to the MEP model.

7.4 Fully nonlinear regime

The fully nonlinear regime is marked by the collapse of the core of the system, the formation of a finite time singularity, and the growth of a Dirac peak by accretion of the surrounding matter in the post-collapse regime. When considering the collapse of the core, one can neglect the pressure as compared to the self-gravity. The core undergoes a self-similar collapse (free fall) in both canonical and

⁷ Of course, in practice, other physical processes such as quantum mechanics and general relativity [39,40] will come into play and prevent this classical mathematical singularity to form. It will be replaced by a quantum compact object such as a white dwarf or a neutron star (if its mass is smaller than the Chandrasekhar [41] or Oppenheimer-Volkoff [42] limit) or by a black hole.

microcanonical ensembles but the exponents are different in the two ensembles. For example, the density profile decreases as $r^{-24/11}$ in the CEP model and as $r^{-48/19}$ in the MEP model. Consequently, in the post-collapse regime, the mass in the Dirac peak increases as $M_c(t) \sim t^{3/4}$ in the CEP model and as $M_c(t) \sim t^{3/8}$ in the MEP model. On the other hand, in the CEP model, the system collapses as a whole while, in the MEP model, it takes a core-halo structure reminiscent of a red giant. The halo is heated by the energy released by the collapsing core and, when considering the evolution of the halo, one can consider that the pressure force overcomes the gravitational attraction. Therefore, the canonical ensemble may be relevant to describe the life and death of supermassive stars which collapse (implode) without exploding (hypernova phenomenon) while the microcanonical ensemble may be relevant to describe the life and death of less massive stars which present a more complex evolution marked by the collapse (implosion) of the core and the explosion of the halo (supernova phenomenon). The final fate of a star is to become a neutron star if its mass is below the Oppenheimer-Volkoff limit or a black hole if its mass is above the Oppenheimer-Volkoff limit.

Remark: In previous works on the statistical mechanics of self-gravitating systems [10,37], the collapse of the system in the microcanonical ensemble was associated with the so-called gravothermal catastrophe. The gravothermal catastrophe is not like an avalanche (or a free fall). During the gravothermal catastrophe the system takes a core-halo structure but remains in hydrostatic equilibrium [43,44]. Its evolution is due to the temperature gradient between the core and the halo and the fact that the core has a negative specific heat $C = dE/dT < 0$ [37,45]. Therefore, by losing heat the core grows hotter and evolves away from equilibrium. On the other hand, the halo does not explode and even barely expands. The evolution of the system consists just in a core collapse. This description applies to globular clusters. During the gravothermal catastrophe their central parts collapse and get hotter while their outer parts are left behind. In our model, which rather applies to gaseous stars described by fluid equations, we are in the opposite regime (see also [38]).⁸ There is no gradient of temperature but the system is not in hydrostatic equilibrium. At low energies and low temperatures, the pressure cannot balance the gravitational attraction and the star collapses. The core experiences a free fall and the halo expands because it is heated by the energy released by the collapsing core (we have adopted a rough energetic constraint where the temperature is uniform but increases with time). We have suggested that this simple model could be related to the onset of red giant structure and to supernova explosions. We note that Lynden-Bell and Wood [37] and Thirring [45] have also related the gravitational instability resulting from the negative spe-

cific heat of self-gravitating systems to the onset of red giant structure and to supernova explosions (see [39] for additional comments). Probably, a realistic model of stars should take into account both energy transfers by temperature gradients as in [43,44] and deviation from hydrostatic equilibrium as in our model.

8 Conclusion

Presently, theories of supernova explosion focus on physical phenomena such as the emission of neutrinos, or complex 3D effects which we do not consider at all in our work. We focus on an entirely different aspect of the physics of supernovae, namely the fluid mechanical part, without considering the immensely complex set of possible nuclear reactions in the core. We show that implosion *and* explosion taking place at the death of a massive star may occur simultaneously. This yields an alternative explanation to the yet unsolved problem of supernova description where the two steps process makes, we believe, an unsatisfactory explanation. Using a simple model which has no aim to reproduce the complex reality of what happens inside a star, we point out first that the huge difference of time scales between the long life of a star and its abrupt death can be understood in the light of a catastrophe-like theory which includes dynamical aspects. This is performed by sweeping slowly a saddle-center bifurcation. Starting from the stable equilibrium state and approaching the saddle-center bifurcation, the weakly nonlinear analysis leads to a universal (Painlevé I) equation followed by a self-similar collapse more rapid than the growing explosion of the outer shell.

It is important to point out that the Painlevé analysis gives access to the sign for the velocity field at the critical point, contrary to what happens in “classical” transitions from a linearly stable to a linearly unstable situation (where the unstable mode may have either positive or negative amplitude). As we have shown, this sign may change as a function of the radius. This fair property of the definite sign of the growing Painlevé solution comes from the fact that in the case of a saddle-center bifurcation, the two stable and unstable equilibrium states (a center and a saddle respectively) merge at the critical point, beyond which no equilibrium state exists (neither stable nor unstable) that makes the difference with the “classical” case.

Our study illustrates once more (see [9]) that a change from canonical to microcanonical description, not looking very important at first, does deeply change the outcome of the transition from stable to unstable state. In the case we have studied, the canonical model collapses without producing any outgoing flow of matter, although the microcanonical model shows a core collapse together with an explosive outer shell. The former case (Paper I) could reproduce what happens in the case of supermassive stars which die via hypernovae showing very intense and directive gamma ray bursts, but no explosion of matter (or a very faint one) and often leads to the formation of black holes. In the present paper, on the other hand, we show that it is possible to reproduce what happens for massive stars which die via supernovae showing explosion of

⁸ This is necessary to account for the very different timescale governing the collapse of globular clusters and stars. The timescale of the gravothermal catastrophe is of the order of the age of the Universe while the timescale of star collapse (e.g. supernova) is of the order of a few days.

matter and often leading to the formation of a neutron star resulting from the core collapse. Therefore, our simple model opens up the way to a new understanding of the explosion of stars, based on fluid mechanics, catastrophe theory, and bifurcation properties of their equilibrium state. It also provides a nice illustration of the property of inequivalence between canonical and microcanonical ensembles for systems with long-range interactions.

The assumption of a uniform temperature inside the star implies physically that heat conduction is very fast so that temperature is made uniform on a time scale much shorter than the one of the physical process we consider. This could be due, for instance, to heat transfer by photons, moving a priori very fast in the star, even though this motion is a kind of Brownian motion, not a straight trajectory. Another physical possibility is given by the well-known Laplace equilibrium in the atmosphere of the Earth: Laplace assumed, rightly, that, because of very fast vertical motions, the air reaches rapidly an isentropic equilibrium, where the entropy per unit mass is constant (notice that the word entropy was absent in Laplace's work, but he understood that fast exchanges like in sound waves are such that there is no irreversible exchange of heat so that the relationship between pressure and volume is given by the relation PV^γ constant, where P is the pressure, V the specific volume, and γ the ratio of heat conductivity at constant pressure and volume). Therefore, if fast vertical motion (likely turbulent) is present in the star, it could be closer to reality to take, instead of a uniform temperature and a global energy conservation, a constraint of Laplace equilibrium, namely a uniform entropy per unit mass together with a conserved total energy. Such an equilibrium with a non uniform temperature is what is expected to represent the present state inside the Sun, with a temperature increasing toward the center. While being not much heavier to treat numerically, this description would be hardly tractable analytically and this is why we considered a simpler isothermal model. However, we expect that, qualitatively, the results should be comparable.

In the description of the halo expansion after the explosion, we made rough approximations. Nevertheless, the points we made clear seem important. In a first stage, we assumed that the halo expands self-similarly powered by the rise of temperature accompanying the contraction of the core. In a second stage, we assumed that the free expansion stage is an isentropic process with two constraints, the conservation of mass and energy. This stage of free expansion, which has not been much studied, reveals itself to be especially interesting because neglecting the gravity with respect to the pressure forces, we find that no self-similar solution exists, contrary to the free fall of dense molecular gas (where the opposite was assumed). Then, we point out that when both pressure and gravity are negligible, another type of solution appears, of Burgers-type, which is a prototype for creating shocks. Such a scenario could happen in the process of remnant expansion, but is not the common one found in the literature which invokes Sedov-Taylor self-similar solutions where the shock is due to the interaction between the remnant and the in-

terstellar matter. Our argument relies on the fact that the mean-free path in interstellar matter may be as large as the size of a galaxy, that makes such event unrealistic. In our rough description shocks are formed naturally inside the remnant, they propagate inside this matter, the role of the interstellar medium being ignored.

Acknowledgement

Two of us (P.H. Chavanis and Y. Pomeau) greatly acknowledge "la fondation des Treilles" which helped finance a colloquium organized in September 2014 in their beautiful mediterranean domain of Tourtour (83690, France) where our collaboration started on this subject.

A Useful relations in original variables

We regroup in this Appendix some useful relations that are needed in our theoretical study. We write the equations in terms of the original (dimensional) variables.

A.1 Newton's law

Integrating the Poisson equation (3) for a spherically symmetric distribution of matter, we obtain Newton's law

$$\Phi_{,r}(r, t) = \frac{GM(r, t)}{r^2}, \quad (181)$$

where

$$M(r, t) = \int_0^r \rho(r', t) 4\pi r'^2 dr' \quad (182)$$

is the mass contained within the sphere of radius r . The density is

$$\rho(r, t) = \frac{M_{,r}(r, t)}{4\pi r^2}. \quad (183)$$

Applying Newton's law at the edge of the star, we get

$$\Phi_{,r}(R(t), t) = \frac{GM}{R(t)^2} \quad \text{and} \quad \Phi(R(t), t) = -\frac{GM}{R(t)}, \quad (184)$$

where M is the total mass of the star (to get the second relation we have assumed that the space is empty outside the star so that Newton's law can be easily integrated for $r \geq R(t)$). For a steady state, using equation (8), the foregoing relations from equations (181) and (184) imply

$$h_{,r}(r) = -\frac{GM(r)}{r^2}, \quad h_{,r}(r_0) = -\frac{GM}{r_0^2}. \quad (185)$$

A.2 Gravitational energy

The gravitational energy of the star is given by

$$W(t) = \frac{1}{2} \int \rho \Phi \, d\mathbf{r}. \quad (186)$$

Using Poisson's equation (3), integrating by parts, and using equation (184) valid for a spherically symmetric distribution of matter, we find that the gravitational energy is given by

$$\begin{aligned} W(t) &= \frac{1}{8\pi G} \int \Phi \Delta \Phi \, d\mathbf{r} \\ &= -\frac{GM^2}{2R(t)} - \frac{1}{8\pi G} \int (\nabla \Phi)^2 \, d\mathbf{r}. \end{aligned} \quad (187)$$

Alternatively, using equation (183), we can write

$$W(t) = \frac{1}{2} \int_0^{R(t)} \rho \Phi 4\pi r^2 \, dr = \frac{1}{2} \int_0^{R(t)} \Phi M_{,r} \, dr. \quad (188)$$

Integrating equation (188) by parts and using equation (184), we obtain

$$W(t) = -\frac{GM^2}{2R(t)} - \frac{1}{2} \int_0^{R(t)} M \Phi_{,r} \, dr. \quad (189)$$

For a steady state, using equation (8), the foregoing equation becomes

$$W = -\frac{GM^2}{2r_0} + \frac{1}{2} \int_0^{r_0} M h_{,r} \, dr. \quad (190)$$

Therefore, at equilibrium, the energy (5) can be written as

$$E = \frac{3}{2} N k_B T - \frac{GM^2}{2r_0} + \frac{1}{2} \int_0^{r_0} M h_{,r} \, dr. \quad (191)$$

A.3 Virial theorem

For a self-gravitating gas in a steady state, the scalar virial theorem writes

$$3 \int P \, d\mathbf{r} + W = 0. \quad (192)$$

Using equation (192), the energy (5) takes the form

$$E = \frac{3}{2} N k_B T - 3 \int P \, d\mathbf{r}. \quad (193)$$

A.4 Radial displacement

We consider a spherically symmetric evolution of the system and define the radial displacement $S(r, t)$ by

$$\delta u = S_{,t}, \quad (194)$$

where $u(r, t)$ is the radial component of the velocity field. In the linearized equations, recalling that the perturbations evolve with time as $e^{\lambda t}$, we get

$$\delta u = \lambda S. \quad (195)$$

The linearized continuity equation (24) may be written as

$$\delta \rho + \frac{1}{r^2} (r^2 \rho S)_{,r} = 0. \quad (196)$$

Multiplying equation (196) by $4\pi r^2$ and integrating between 0 and r , we get

$$S(r) = -\frac{\delta M(r)}{4\pi \rho(r) r^2}. \quad (197)$$

This relation is valid for $r < r_0$. It is undetermined at $r = r_0$ where $\rho = 0$. However, coming back to equation (196), and expanding the derivative, we obtain

$$S(r_0) = -\frac{\delta \rho(r_0)}{\rho_{,r}(r_0)}. \quad (198)$$

B Useful relations in scaled variables at the critical point

In this Appendix, we regroup some useful relations in scaled variables that we apply at the critical point. In all the subsequent formulae, we suppress the hats (in the final equations) in order to simplify the notations.

Writing equation (31) in scaled variables, we get

$$j_{,r}(r) = -\delta \Phi_{,r}^{(c)}(r) = -\frac{\delta M^{(c)}(r)}{r^2}. \quad (199)$$

Since $\delta M^{(c)}(r_c) = 0$ because the total mass is conserved, the foregoing equation gives $j_{,r}(r_c) = 0$. Knowing $j(r)$ we obtain $\delta M^{(c)}(r)$ by the relation

$$\delta M^{(c)}(r) = -r^2 j_{,r}(r). \quad (200)$$

Writing equation (183) in perturbed form and introducing the scaled variables, we get

$$\delta \rho^{(c)}(r) = \frac{\delta M_{,r}^{(c)}}{4\pi r^2} = -\frac{1}{4\pi} \Delta j, \quad (201)$$

where we have used equation (200) to obtain the last equality. Writing equation (197) in scaled variables with $\hat{S} = S/T^{1/2}$, we get

$$S^{(c)}(r) = -\frac{\delta M^{(c)}(r)}{4\pi \rho^{(c)}(r) r^2} = \frac{j_{,r}(r)}{4\pi \rho^{(c)}(r)}, \quad (202)$$

where we have used equation (200) to obtain the last equality. At the edge of the star, writing equations (38) and (198) in scaled variables, we get

$$S^{(c)}(r_c) = -\frac{\delta \rho^{(c)}(r_c)}{\rho_{,r}^{(c)}(r_c)} = -\frac{2j(r_c)}{\rho_{,r}^{(c)}(r_c)}. \quad (203)$$

C A self-similar solution for the expansion of the halo

In this Appendix, we construct a self-similar solution describing the expansion of the halo according to the model developed in Section 5.2.

C.1 Euler equations

We consider the Euler equations

$$\frac{\partial \rho}{\partial t} + \nabla \cdot (\rho \mathbf{u}) = 0, \quad (204)$$

$$\frac{\partial \mathbf{u}}{\partial t} + (\mathbf{u} \cdot \nabla) \mathbf{u} = -\frac{1}{\rho} \nabla P, \quad (205)$$

with a polytropic equation of state of the form

$$P = K(t) \rho^\gamma, \quad (206)$$

where $K(t)$ is a given function of time. We assume that $K(t) \geq 0$ in order to have a positive pressure. We assume that $\gamma > 0$ so that the pressure force leads to an expansion of the halo: $-(1/\rho)P'(\rho)d\rho/dr > 0$ (recalling that $d\rho/dr < 0$). Finally, we neglect the self-gravity of the halo in equation (206), an approximation whose validity will be discussed in Section C.4.

C.2 Scaling ansatz

We look for a self-similar solution of equations (204)-(206) of the form

$$\rho(\mathbf{r}, t) = \frac{M}{R(t)^3} f\left[\frac{\mathbf{r}}{R(t)}\right], \quad \mathbf{u}(\mathbf{r}, t) = H(t) \mathbf{r}. \quad (207)$$

We have assumed that the velocity field is proportional to the radial distance \mathbf{r} with a proportionality factor $H(t)$. Defining

$$\mathbf{x} = \frac{\mathbf{r}}{R(t)}, \quad (208)$$

we can rewrite equation (207) as

$$\rho(\mathbf{r}, t) = \frac{M}{R(t)^3} f(\mathbf{x}), \quad \mathbf{u}(\mathbf{r}, t) = H(t) R(t) \mathbf{x}. \quad (209)$$

In the foregoing equations $R(t)$ is the typical size (radius) of the halo and $f(\mathbf{x})$ is the invariant density profile. We assume that the density profile contains all the mass ($\int \rho(\mathbf{r}, t) d\mathbf{r} = M$) so that $\int f(\mathbf{x}) d\mathbf{x} = 1$.

The continuity equation (204) can be rewritten as

$$\frac{\partial \ln \rho}{\partial t} + \nabla \cdot \mathbf{u} + \mathbf{u} \cdot \nabla \ln \rho = 0. \quad (210)$$

From equation (207), we obtain

$$\begin{aligned} \frac{\partial \ln \rho}{\partial t} &= -\frac{\dot{R}}{R} \mathbf{x} \cdot \nabla_{\mathbf{x}} \ln f - 3 \frac{\dot{R}}{R}, \\ \nabla \ln \rho &= \frac{1}{R} \nabla_{\mathbf{x}} \ln f, \quad \nabla \cdot \mathbf{u} = 3H. \end{aligned} \quad (211)$$

Substituting the foregoing relations into equation (210), we get

$$\left(H - \frac{\dot{R}}{R}\right) (3 + \mathbf{x} \cdot \nabla_{\mathbf{x}} \ln f) = 0. \quad (212)$$

This equation must be satisfied for all \mathbf{x} . This implies

$$H(t) = \frac{\dot{R}}{R}. \quad (213)$$

We note the formal analogy with the Hubble constant in cosmology. We have $\mathbf{u}(\mathbf{r}, t) = [\dot{R}/R(t)] \mathbf{r} = \dot{R} \mathbf{x}$.

Using equation (207), the left hand side of the Euler equation (205) can be written as

$$\frac{\partial \mathbf{u}}{\partial t} + (\mathbf{u} \cdot \nabla) \mathbf{u} = (\dot{H} + H^2) \mathbf{r} = \frac{\ddot{R}}{R} \mathbf{r} = \ddot{R} \mathbf{x}. \quad (214)$$

For an equation of state of the form of equation (206), the pressure term in the right hand side of equation (205) is given by

$$-\frac{1}{\rho} \nabla P = -K(t) \gamma \rho^{\gamma-2} \nabla \rho. \quad (215)$$

With the scaling ansatz from equation (207), we obtain

$$-\frac{1}{\rho} \nabla P = -K(t) \gamma \frac{M^{\gamma-1}}{R^{3\gamma-2}} f^{\gamma-2} \nabla_{\mathbf{x}} f. \quad (216)$$

Substituting equations (214) and (216) into the Euler equation (205), and assuming that f depends only on $x = |\mathbf{x}|$, we get

$$\ddot{R} = -K(t) \gamma \frac{M^{\gamma-1}}{R^{3\gamma-2}} f^{\gamma-2} \frac{f'(x)}{x}. \quad (217)$$

The variables of position and time separate provided that

$$f^{\gamma-2} \frac{df}{dx} + 2Ax = 0 \quad (218)$$

and

$$\ddot{R} = 2AK(t) \gamma \frac{M^{\gamma-1}}{R^{3\gamma-2}}, \quad (219)$$

where A is a constant (the factor 2 has been introduced for convenience). These differential equations determine the invariant halo profile $f(x)$ and the evolution of the halo radius $R(t)$.

C.3 Invariant halo profile and halo radius

The differential equation (218) determining the invariant profile of the halo can be integrated into

$$f(x) = [C - (\gamma - 1)Ax^2]_+^{1/(\gamma-1)}, \quad (220)$$

where $[x]_+ = x$ if $x \geq 0$ and $[x]_+ = 0$ if $x \leq 0$. Therefore, the invariant profile (220) is given by a Tsallis distribution [27] of index γ (see Section VI of [46]). We can take $C = A$ without loss of generality. Denoting this constant by $Z^{1-\gamma}$, we get

$$f(x) = \frac{1}{Z} [1 - (\gamma - 1)x^2]_+^{1/(\gamma-1)}, \quad (221)$$

where Z is determined by the normalization condition $\int f(\mathbf{x}) d\mathbf{x} = 1$. This yields

$$Z = \int_0^{x_{\max}} [1 - (\gamma - 1)x^2]_+^{1/(\gamma-1)} 4\pi x^2 dx, \quad (222)$$

where $x_{\max} = 1/\sqrt{\gamma - 1}$ if $\gamma \geq 1$ and $x_{\max} = +\infty$ if $1/3 < \gamma \leq 1$. The distribution is not normalizable when $\gamma \leq 1/3$. Therefore, in the following, we assume $\gamma > 1/3$. The integral can be expressed in terms of Gamma functions leading to

$$Z = \frac{\pi^{3/2} \Gamma\left(\frac{1}{\gamma-1}\right)}{(\gamma-1)^{5/2} \Gamma\left(\frac{3}{2} + \frac{\gamma}{\gamma-1}\right)} \quad (\gamma \geq 1), \quad (223)$$

$$Z = \frac{\pi^{3/2} \Gamma\left(\frac{1}{1-\gamma} - \frac{3}{2}\right)}{(1-\gamma)^{3/2} \Gamma\left(\frac{1}{1-\gamma}\right)} \quad (1/3 < \gamma \leq 1). \quad (224)$$

On the other hand, the differential equation (219) determining the evolution of the halo radius becomes

$$\ddot{R} = 2Z^{1-\gamma} K(t) \gamma \frac{M^{\gamma-1}}{R^{3\gamma-2}}. \quad (225)$$

By a proper rescaling, we can write this equation as

$$\ddot{R} R^{3\gamma-2} = K(t). \quad (226)$$

For the isothermal equation of state $P = \rho k_B T(t)/m$ (corresponding to $\gamma = 1$), the invariant halo profile is the Gaussian

$$f(x) = \frac{1}{\pi^{3/2}} e^{-x^2} \quad (227)$$

and the evolution of the halo radius is determined by a differential equation of the form

$$\ddot{R} = \frac{T(t)}{R}. \quad (228)$$

For the polytropic equation of state $P = K(t)\rho^2$ (corresponding to $\gamma = 2$), the invariant halo profile is parabolic

$$f(x) = \frac{15}{8\pi} (1 - x^2)_+ \quad (229)$$

and the evolution of the halo radius is determined by a differential equation of the form

$$\ddot{R} = \frac{K(t)}{R^4}. \quad (230)$$

We note that the expansion of the halo is always accelerating ($\ddot{R} > 0$).

C.4 Validity of the approximations

The Euler equations (204) and (205) are valid provided that we can neglect the self-gravity of the halo as compared to the pressure force. The pressure force scales as

$$\frac{1}{\rho} |\nabla P| = \frac{1}{\rho} K(t) |\nabla \rho^\gamma| \sim \frac{K(t) \rho^{\gamma-1}}{R} \sim \frac{K(t) M^{\gamma-1}}{R^{3\gamma-2}}, \quad (231)$$

while the gravitational force scales as

$$|\nabla \Phi| \sim \frac{GM}{R^2}. \quad (232)$$

Therefore, when R is large, the gravitational force is negligible in front of the pressure force provided that

$$\frac{GM}{R^2} \ll \frac{K(t) M^{\gamma-1}}{R^{3\gamma-2}}. \quad (233)$$

The validity of this approximation depends on the function $K(t)$ and on the value of the polytropic index γ . Some examples are given below.

C.5 The case $K(t) = 1$

In this subsection, we assume that the temperature is constant:

$$K(t) = 1. \quad (234)$$

In that case, the differential equation (226) becomes

$$\ddot{R} = \frac{1}{R^{3\gamma-2}}. \quad (235)$$

It is similar to the fundamental equation of dynamics (Newton's equation) for a fictive particle of unit mass and position $R(r)$ submitted to a repulsive force of the form $F = 1/R^{3\gamma-2}$. The case of an arbitrary polytropic index γ is treated in Ref. [28] by developing an analogy with the Friedmann equations of cosmology.

C.5.1 Isothermal equation of state ($\gamma = 1$)

Here, we specifically consider the case $\gamma = 1$ corresponding to an isothermal equation of state. In that case, the differential equation (235) becomes

$$\ddot{R} = \frac{1}{R}. \quad (236)$$

It can be written as

$$\ddot{R} = -\frac{dV}{dR} \quad \text{with} \quad V(R) = -\ln R. \quad (237)$$

The first integral of motion is

$$E = \frac{1}{2} \left(\frac{dR}{dt} \right)^2 + V(R), \quad (238)$$

where E is a constant. The evolution of the halo radius $R(t)$ is therefore determined by the integral

$$t = \int_{R_0}^{R(t)} \frac{dR}{\sqrt{2(E - V(R))}}, \quad (239)$$

where R_0 is its value at $t = 0$. In writing equation (239) we have assumed that $R(t)$ always increases with time. Substituting the potential $V(R)$ from equation (237) into equation (239), we obtain

$$t = \int_{R_0}^{R(t)} \frac{dR}{\sqrt{2(E + \ln R)}}. \quad (240)$$

Making the change of variables $x = \sqrt{E + \ln R}$ in equation (240), we get

$$t = \sqrt{2}e^{-E} \int_{\sqrt{E + \ln R_0}}^{\sqrt{E + \ln R(t)}} e^{x^2} dx. \quad (241)$$

This equation can be rewritten as

$$t = \sqrt{2}R(t)D(\sqrt{E + \ln R(t)}) - \sqrt{2}R_0D(\sqrt{E + \ln R_0}), \quad (242)$$

where $D(x)$ is Dawson's function

$$D(x) = e^{-x^2} \int_0^x e^{t^2} dt. \quad (243)$$

It has the asymptotic behavior

$$D(x) = \frac{1}{2x} + \frac{1}{4x^3} + \dots \quad (x \rightarrow +\infty). \quad (244)$$

Therefore, for $t \rightarrow +\infty$, we obtain

$$t \sim \frac{R}{\sqrt{2 \ln R}}, \quad (245)$$

leading to (at leading order):

$$R(t) \sim t\sqrt{2 \ln t}. \quad (246)$$

The radius of the halo expands linearly in time with a logarithmic correction. The velocity of expansion

$$\dot{R}(t) \sim \sqrt{2 \ln t}, \quad \dot{R}^2(t) \sim 2 \ln t \quad (247)$$

increases logarithmically in time.

C.5.2 Asymptotic results for an arbitrary index

Here, we provide asymptotic results valid when $t \rightarrow +\infty$. For an arbitrary index γ , the potential writes

$$V(R) = \frac{1}{3(\gamma - 1)} \frac{1}{R^{3(\gamma - 1)}}. \quad (248)$$

We first assume $\gamma > 1$. For $R \rightarrow +\infty$, the potential $V(R) \rightarrow 0$ and the first integral of motion (238) reduces to $\dot{R} \sim \sqrt{2E}$ (with $E > 0$) leading to

$$R(t) \sim \sqrt{2E} t \quad (t \rightarrow +\infty). \quad (249)$$

We now assume $1/3 < \gamma < 1$. For $R \rightarrow +\infty$, the potential $V(R) \rightarrow -\infty$ and the first integral of motion (238) reduces to $\dot{R} \sim \sqrt{-2V(R)}$ leading to

$$R(t) \sim \left[\frac{(3\gamma - 1)^2}{6(1 - \gamma)} \right]^{1/(3\gamma - 1)} t^{2/(3\gamma - 1)} \quad (t \rightarrow +\infty). \quad (250)$$

For $K(t) = 1$ the condition of validity of our study (233) takes the form $R^{4-3\gamma} \gg 1$. Since $R(t) \rightarrow +\infty$ for $t \rightarrow +\infty$, the foregoing asymptotic behaviors are valid provided that $\gamma < 4/3$.

C.6 The case $K(t) = t^a$ (post-collapse)

In this subsection, we assume that the temperature evolves with time as a power law:

$$K(t) = t^a. \quad (251)$$

In that case, the differential equation (226) becomes

$$\ddot{R} R^{3\gamma - 2} = t^a. \quad (252)$$

For the sake of generality, we let the value of a arbitrary (positive or negative). For $a > 0$ the temperature increases with time up to infinity. This is the situation corresponding to the post-collapse regime considered in Section 5 where $a = 3/8$ and $\gamma = 1$ (isothermal gas). For $a < 0$ the temperature decreases with time up to zero.

C.6.1 Solution $R(t) = At^q$ with $q > 0$

We consider a solution of equation (252) of the form

$$R(t) = At^q \quad (253)$$

with $q > 0$ (and, of course, $A > 0$). In that case, the halo radius increases with time up to infinity. Substituting this ansatz into equation (252) we get

$$Aq(q - 1)t^{q-2} A^{3\gamma - 2} t^{(3\gamma - 2)q} = t^a, \quad (254)$$

implying

$$q = \frac{a + 2}{3\gamma - 1} \quad (255)$$

and

$$A^{3\gamma-1} = \frac{1}{q(q-1)}. \quad (256)$$

Considering equation (256), and recalling that $q > 0$ and $A > 0$, we see that a necessary condition for the existence of a solution is that $q > 1$. Considering equation (255) with $q > 1$, and recalling that $\gamma > 1/3$, we find that the solution exists provided that $a > -2$ and $1/3 < \gamma < (a+3)/3$.

The condition of validity of our study (233) takes the form

$$\frac{1}{t^{2q}} \ll \frac{t^a}{t^{(3\gamma-2)q}} \quad \text{for} \quad t \rightarrow +\infty. \quad (257)$$

When $\gamma > 1/3$ this requires $\gamma < (3a+8)/6$. This condition is always satisfied when the solution exists. When $a = 0$ the solution exists and is valid provided that $1/3 < \gamma < 1$. When $\gamma = 1$ the solution exists and is valid provided that $a > 0$. When $\gamma = 1$ and $a = 3/8$ (see Section 5), we get $R = (16/\sqrt{57})t^{19/16}$, which is close to the law $R \sim vt$ corresponding to a constant kinetic energy (see Section 6).

Remark: There exist solutions where the radius increases with time ($q > 0$) while the temperature decreases with time ($a < 0$).

C.6.2 Solution $R(t) = At^q$ with $q < 0$

We consider a solution of equation (252) of the form of equation (253) with $q < 0$ (and, of course, $A > 0$). In that case, the halo radius decreases with time up to zero. Substituting this ansatz into equation (252) we get equation (254) implying equations (255) and (256). Considering equation (255) with $q < 0$, and recalling that $\gamma > 1/3$, we find that the solution exists provided that $a < -2$.

The condition of validity of our study (233) takes the form of equation (257). When $\gamma > 1/3$ this requires $\gamma < (3a+8)/6$. This condition is never fulfilled when the solution exists. When $a = 0$ the solution does not exist. When $\gamma = 1$ the solution exists provided that $a < -2$ but it is not valid.

C.6.3 Asymptotic solution $\dot{R}(t) \rightarrow v$ with $v > 0$

We consider an asymptotic solution of equation (252) of the form

$$R(t) = vt + \epsilon(t) \quad (258)$$

with $v > 0$ and $|\epsilon(t)| \ll vt$ for $t \rightarrow +\infty$. This means that the velocity \dot{R} of the halo (or its kinetic energy $\propto \dot{R}^2$) tends to a constant for large times. Substituting this ansatz into equation (252) we get for $t \gg 1$:

$$\ddot{\epsilon} \sim \frac{1}{v^{3\gamma-2}} t^{a-3\gamma+2}. \quad (259)$$

After two integrations, we obtain (the constants of integration can be taken equal to zero without restriction of generality)

$$\epsilon(t) \sim \frac{1}{v^{3\gamma-2}} \frac{t^{a-3\gamma+4}}{(a-3\gamma+3)(a-3\gamma+4)}. \quad (260)$$

The velocity of the halo is

$$\dot{R} \simeq v + \frac{1}{v^{3\gamma-2}} \frac{t^{a-3\gamma+3}}{a-3\gamma+3}. \quad (261)$$

Note that the terminal velocity v cannot be determined by this asymptotic approach as it depends on the initial condition. The condition $|\epsilon(t)| \ll vt$ for $t \rightarrow +\infty$ impose $\gamma > (a+3)/3$. Since our approach assumes $\gamma > 1/3$, we find that the solution exists (i) for any $\gamma > 1/3$ when $a < -2$; (ii) for $\gamma > (a+3)/3$ when $a > -2$.

The condition of validity of our study (233) takes the form

$$\frac{1}{t^2} \ll \frac{t^a}{t^{3\gamma-2}} \quad \text{for} \quad t \rightarrow +\infty. \quad (262)$$

This requires $\gamma < (a+4)/3$. We note in that case that $\epsilon(t) < 0$ so that asymptotically $R(t) \lesssim vt$. In conclusion, the solution exists and is valid provided that (i) $-3 < a < -2$ and $1/3 < \gamma < (a+4)/3$; (ii) $a > -2$ and $(a+3)/3 < \gamma < (a+4)/3$. When $a = 0$ the solution exists and is valid provided that $1 < \gamma < 4/3$. When $\gamma = 1$ the solution exists and is valid provided that $-1 < a < 0$.

Remark: There exist solutions where the radius increases with time while the temperature decreases with time ($a < 0$).

C.6.4 Asymptotic solution $R(t) \sim (t_f - t)^q$ with $q < 0$

We consider an asymptotic solution of equation (252) of the form

$$R(t) \sim A(t_f - t)^q \quad (263)$$

with $q < 0$ (and, of course, $A > 0$). This corresponds to a future finite time singularity in the sense that the halo radius becomes infinite in a finite time t_f . Defining $\tau = t_f - t$ and substituting this ansatz into equation (252), we get for $\tau \rightarrow 0$:

$$Aq(q-1)\tau^{q-2}A^{3\gamma-2}\tau^{q(3\gamma-2)} \sim t_f^a, \quad (264)$$

implying

$$q = \frac{2}{3\gamma-1} \quad (265)$$

and

$$A^{3\gamma-1} = \frac{t_f^a}{q(q-1)}. \quad (266)$$

Considering equation (265) and recalling that $\gamma > 1/3$, we find that the condition $q < 0$ is never fulfilled. Therefore, there is no solution of that form.

C.6.5 Asymptotic solution $R(t) \sim (t_f - t)^q$ with $q > 0$

We consider an asymptotic solution of equation (252) of the form of equation (263) with $q > 0$ (and, of course, $A > 0$). In that case, the halo radius vanishes in a finite time t_f . Defining $\tau = t_f - t$ and substituting this ansatz into equation (252), we get equation (264) for $\tau \rightarrow 0$, implying equations (265) and (266). Considering equation (266), and recalling that $q > 0$ and $A > 0$, we see that a necessary condition for the existence of a solution is that $q > 1$. Considering equation (265) with $q > 1$, we find that the solution exists provided that $1/3 < \gamma < 1$, independently of a .

The condition of validity of our study (233) takes the form

$$\tau^{-2q} \ll \tau^{-(3\gamma-2)q} \quad \text{for} \quad \tau \rightarrow 0. \quad (267)$$

This requires $\gamma > 4/3$. This condition is never fulfilled when the solution exists. When $a = 0$ the solution exists provided that $1/3 < \gamma < 1$ but it is not valid. There is no solution of the form (263) when $\gamma = 1$.

C.6.6 Conclusions

Regrouping the foregoing results, and considering only solutions that satisfy the condition of validity of our study (233), we come to the following conclusions: (i) When $-3 < a < -2$ the solution of equation (252) behaves asymptotically as $R \sim vt$ for $1/3 < \gamma < (a+4)/3$ (see Appendix C.6.3); (ii) When $a > -2$ the solution of equation (252) behaves asymptotically as $R \sim At^q$ with $q > 0$ for $1/3 < \gamma < (a+3)/3$ (see Appendix C.6.1) and as $R \sim vt$ for $(a+3)/3 < \gamma < (a+4)/3$ (see Appendix C.6.3).

When $a = 0$, the solution of equation (252) behaves asymptotically as $R \sim At^{2/(3\gamma-1)}$ for $1/3 < \gamma < 1$ (see Appendices C.5.2 and C.6.1), as $R \sim t\sqrt{2\ln t}$ for $\gamma = 1$ (see Appendix C.5.1), and as $R \sim vt$ for $1 < \gamma < 4/3$ (see Appendices C.5.2 and C.6.3).

When $\gamma = 1$, the solution of equation (252) behaves asymptotically as $R \sim vt$ for $-1 < a < 0$ (see Appendix C.6.3), as $R \sim t\sqrt{2\ln t}$ for $a = 0$ (see Appendix C.5.1), and as $R \sim At^{(a+2)/2}$ for $a > 0$ (see Appendix C.6.1).

When $a = 3/8$ and $\gamma = 1$, which is the situation corresponding to the post-collapse regime considered in Section 5, the solution of equation (252) behaves asymptotically as $R \sim At^{19/16}$ (see Appendix C.6.1).

C.7 The case $K(t) = (t_{\text{coll}} - t)^a$ (pre-collapse)

In this subsection, we assume that the temperature behaves as

$$K(t) = (t_{\text{coll}} - t)^a. \quad (268)$$

In that case, the differential equation (226) becomes

$$\ddot{R}R^{3\gamma-2} = (t_{\text{coll}} - t)^a. \quad (269)$$

Defining $\tau = t_{\text{coll}} - t$, it reduces to

$$\ddot{R}R^{3\gamma-2} = \tau^a. \quad (270)$$

For the sake of generality, we let the value of a arbitrary (negative or positive). When $a < 0$, the temperature diverges in a finite time t_{coll} . This is the situation corresponding to the pre-collapse regime considered in Section 4 where $a = -1/24$ and $\gamma = 1$ (isothermal gas). When $a > 0$, the temperature tends to zero in a finite time t_{coll} .

C.7.1 Solution $R(\tau) = A(t_{\text{coll}} - t)^q$ with $q < 0$

We consider a solution of equation (269) of the form

$$R(\tau) = A\tau^q \quad (271)$$

with $q < 0$ (and, of course, $A > 0$). In that case, the radius $R(t)$ increases and becomes infinite at $t = t_{\text{coll}}$. Substituting this ansatz into equation (270) we get

$$Aq(q-1)\tau^{q-2}A^{3\gamma-2}\tau^{(3\gamma-2)q} = \tau^a, \quad (272)$$

implying

$$q = \frac{a+2}{3\gamma-1} \quad (273)$$

and

$$A^{3\gamma-1} = \frac{1}{q(q-1)}. \quad (274)$$

Considering equation (273) with $q < 0$, and recalling that $\gamma > 1/3$, we find that the solution exists provided that $a < -2$.

The condition of validity of our study (233) takes the form

$$\frac{1}{\tau^{2q}} \ll \frac{\tau^a}{\tau^{(3\gamma-2)q}} \quad \text{for} \quad \tau \rightarrow 0. \quad (275)$$

When $\gamma > 1/3$ this requires $\gamma > (3a+8)/6$. This condition is always fulfilled when the solution exists. When $a = 0$ the solution does not exist. When $\gamma = 1$ the solution exists and is valid provided that $a < -2$. For the case considered in Section 4.2, corresponding to $\gamma = 1$ and $a = -1/24$, the condition $a < -2$ is not satisfied so there is no solution of the form of equation (271) with $q < 0$. This suggests that the radius of the halo does not diverge at t_{coll} in agreement with the numerical solution of the MEP model.

C.7.2 Solution $R(\tau) = A(t_{\text{coll}} - t)^q$ with $q > 0$

We consider a solution of equation (269) of the form of equation (271) with $q > 0$ (and, of course, $A > 0$). In that case, the radius $R(t)$ decreases and tends to zero at $t = t_{\text{coll}}$. Substituting this ansatz into equation (270) we get equation (272) implying equations (273) and (274). Considering equation (274), and recalling that $q > 0$ and

$A > 0$, we see that a necessary condition for the existence of a solution is that $q > 1$. Considering equation (273) with $q > 1$, and recalling that $\gamma > 1/3$, we find that the solution exists provided that $a > -2$ and $1/3 < \gamma < (a+3)/3$.

The condition of validity of our study (233) takes the form of equation (275). When $\gamma > 1/3$ this requires $\gamma > (3a+8)/6$. This condition is never fulfilled when the solution exists. For the case considered in Section 4.2, corresponding to $\gamma = 1$ and $a = -1/24 > -2$, the condition $1/3 < \gamma < (a+3)/3 = 71/72$ is not satisfied, so there is no solution of the form of equation (271) with $q > 1$ (we get $q = 47/48 < 1$). This suggests that the radius of the halo does not tend to zero at t_{coll} in agreement with the numerical solution of the MEP model.

C.7.3 Asymptotic solution $R(t) \rightarrow B$

We consider an asymptotic solution of equation (269) of the form

$$R(\tau) = B + \epsilon(\tau) \quad (276)$$

with $|\epsilon(\tau)| \rightarrow 0$ when $\tau \rightarrow 0$. In that case, the radius $R(t)$ reaches a finite value B at $t = t_{\text{coll}}$. Substituting this ansatz into equation (270) we get for $\tau \ll 1$:

$$\ddot{\epsilon} \sim \frac{1}{B^{3\gamma-2}} \tau^a. \quad (277)$$

After two integrations, we obtain

$$\epsilon(t) \sim \frac{1}{B^{3\gamma-2}} \frac{\tau^{a+2}}{(a+2)(a+1)} - v\tau, \quad (278)$$

where v is a constant of integration (the other constant of integration can be taken equal to zero without restriction of generality). This solution exists provided that $a > -2$. We note that B and v cannot be determined by this asymptotic approach since they depend on the initial condition. The velocity of expansion is

$$\dot{R}(t) = -\dot{R}(\tau) = -\dot{\epsilon}(\tau) \sim -\frac{1}{B^{3\gamma-2}} \frac{\tau^{a+1}}{a+1} + v. \quad (279)$$

When $a > -1$, the velocity $\dot{R}(t)$ tends to a finite value v at t_{coll} . When $a < -1$, the velocity $\dot{R}(t)$ tends to $+\infty$ as $t \rightarrow t_{\text{coll}}$.

The condition of validity of our study (233) takes the form

$$1 \ll \tau^a \quad \text{for} \quad \tau \rightarrow 0. \quad (280)$$

This condition is fulfilled provided that $a < 0$. In conclusion, the solution exists and is valid provided that $-2 < a < 0$. When $a = 0$ the solution exists but is not valid. When $\gamma = 1$ the solution exists and is valid provided that $-2 < a < 0$. For the case considered in Section 4.2, corresponding to $\gamma = 1$ and $a = -1/24$, we find that the solution (276) exists and is valid. Together with the result of Appendices C.7.1 and C.7.2, this strongly suggests that the radius of the halo tends to a constant at $t = t_{\text{coll}}$ in agreement with the numerical solution of the MEP model. Furthermore, since $a = -1/24 > -1$, the velocity $\dot{R}(t)$ tends to a finite value v at $t = t_{\text{coll}}$.

C.7.4 Conclusions

Regrouping the foregoing results, and considering only solutions that satisfy the condition of validity of our study (233), we come to the following conclusions: (i) When $a < -2$ the solution of equation (269) behaves asymptotically as $R \sim A(t_{\text{coll}} - t)^q$ with $q < 0$ for $\gamma > 1/3$ (see Appendix C.7.1); (ii) When $-2 < a < 0$ the solution of equation (269) tends to a constant $R \rightarrow B$ for $\gamma > 1/3$ (see Appendix C.7.3).

When $\gamma = 1$, the solution of equation (269) behaves asymptotically as $R \sim A(t_{\text{coll}} - t)^{(a+2)/2}$ for $a < -2$ (see Appendix C.7.1) and tends to a constant $R \rightarrow B$ for $-2 < a < 0$ (see Appendix C.7.3).

When $a = -1/24$ and $\gamma = 1$, which is the situation corresponding to the pre-collapse regime considered in Section 4, the solution of equation (269) tends to a constant $R \rightarrow B$ (see Appendix C.7.3).

References

1. H.A. Bethe, Rev. Mod. Phys. **62**, 801 (1990).
2. A. Burrows, Rev. Mod. Phys. **85**, 245 (2013).
3. Y. Pomeau, M. Le Berre, P.H. Chavanis, B. Denet, Eur. Phys. J. E **37**, 26 (2014).
4. Y. Pomeau, M. Le Berre, C. Narteau, P. Fromy, in *Comptes-rendus de la 14ème Rencontre du Non-Linéaire*, edited by C. Josserand et al. (Paris 2011), 135-144; Y.Pomeau, M. Le Berre, arXiv:1102.5637.
5. R. D. Peters, M. Le Berre, Y. Pomeau, Phys. Rev. E **86**, 026207 (2012).
6. A. J. K. Phillips, P. A. Robinson, Phys. Rev. E **79**, 021913 (2009).
7. Y. Pomeau, M. Le Berre, Chaos, CNN, in *Memristors and Beyond*, Special Issue in honor of Léon Chua (A. Adamatzky, G. Chen Eds.), Chap. 28 (World Scientific, 2012).
8. Y. Pomeau, M. Le Berre, arXiv:1107.3331.
9. P.H. Chavanis, Int. J. Mod. Phys. B **20**, 3113 (2006).
10. V.A. Antonov, Vest. Leningr. Gos. Univ. **7**, 135 (1962) [translation in IAU symposium **113**, 525 (1985)].
11. M. Hénon Ann. Astrophys. **24**, 369 (1961).
12. M.L. Chabanol, F. Corson, Y. Pomeau, Europhys. Lett. **50**, 148 (2000).
13. Y. Pomeau "Statistical Mechanics of Gravitational Plasma", in *Proceedings of 2nd Warsaw School of Statistical physics* (University of Warsaw Press, 2008), 165-207.
14. P.H. Chavanis, Astron. Astrophys. **556**, A93 (2013).
15. M. Le Berre, Y. Pomeau, P.H. Chavanis, B. Denet "Supernova: Explosion or Implosion?", in *Comptes-rendus de la 17ème Rencontre du Non-Linéaire*, edited by E. Falcon, M. Lefranc, F. Pétrélis, C.T. Pham (Paris 2014).
16. R. Emden, *Gaskugeln Anwendungen der Mechanischen Wärmetheorie auf Kosmologische und Meteorologie Probleme* (Teubner, Leipzig, 1907).
17. S. Chandrasekhar, *An Introduction to the Theory of Stellar Structure* (Dover, 1942).
18. P.H. Chavanis, Astron. Astrophys. **381**, 340 (2002).
19. H. Poincaré, Acta Math. **7**, 259 (1885).
20. J. Katz, Mon. Not. R. Astron. Soc. **183**, 765 (1978).

21. H. Nessyahu, E. Tadmor, J. Comput. Phys. **87**, 408 (1990).
22. J. Balbas, E. Tadmor, CentPack, <http://www.cscamm.umd.edu/centpack>.
23. Z.G.I. Barenblatt, Y. B. Zel'dovich, Ann. Rev. Fluid Mech. **4**, 285 (1972).
24. M.V. Penston, Mon. Not. R. Astron. Soc. **144**, 425 (1969).
25. C. Josserand, Y. Pomeau, S. Rica, J. Low Temp. Phys. **145**, 231 (2006).
26. J. Sopik, C. Sire, P.H. Chavanis, Phys. Rev. E **74**, 011112 (2006).
27. C. Tsallis, J. Stat. Phys. **52**, 479 (1988).
28. P.H. Chavanis, in preparation.
29. L. Spitzer, *Diffuse Matter in Space* (Wiley, N. Y., 1968).
30. L. Spitzer, *Physical Processes in the Interstellar Medium* (Wiley, N.Y., 1977).
31. L.D. Landau, E.M. Lifshitz, *Fluid Mechanics*, Course of Theoretical Physics (Pergamon, Oxford, 1987).
32. L.I. Sedov, J. Appl. Math. Mech. **10**, 241 (1946).
33. R. Latter, J. Appl. Phys. **26**, 954 (1955).
34. J. Lockwood-Taylor, Phil. Mag. **46**, 317 (1955).
35. M.J. Klein, *Principles of the Theory of Heat* (D. Reidel Pub. Cy., Dordrecht, 1986).
36. G. Ranque, J. Phys. Rad. **4**, 112 (1933).
37. D. Lynden-Bell, R. Wood, Mon. Not. R. Astron. Soc. **138**, 495 (1968).
38. C. Sire, P.H. Chavanis, Phys. Rev. E **66**, 046133 (2002).
39. G. Alberti, P.H. Chavanis, arXiv:1808.01007.
40. Z. Roupas, P.H. Chavanis, Class. Quantum Grav. **36**, 065001 (2019).
41. S. Chandrasekhar, Astrophys. J. **74**, 81 (1931).
42. J.R. Oppenheimer, G.M. Volkoff, Phys. Rev. **55**, 374 (1939).
43. D. Lynden-Bell, P.P. Eggleton, Mon. Not. R. Astron. Soc. **191**, 483 (1980).
44. S. Inagaki, D. Lynden-Bell, Mon. Not. R. Astron. Soc. **205**, 913 (1983).
45. W. Thirring, Z. Physik **235**, 339 (1970).
46. C. Sire, P.H. Chavanis, Phys. Rev. E **78**, 061111 (2008).